PHYSICAL REVIEW D **94,** 095006 (2016)

WWV $(V=\gamma, Z)$ vertex in the Georgi-Machacek model

M. A. Arroyo-Ureña, G. Hernández-Tomé, and G. Tavares-Velasco
Facultad de Ciencias Físico Matemáticas, Benemérita Universidad Autónoma de Puebla, Apartado postal 1152, 72001 Puebla, Pue., México
(Received 6 September 2016; published 4 November 2016)

The CP-even static form factors $\Delta\kappa'_V$ and ΔQ_V ($V=\gamma, Z$) associated with the WWV vertex are studied in the context of the Georgi-Machacek model (GMM), which predicts nine new scalar bosons accommodated in a singlet, a triplet, and a fiveplet. General expressions for the one-loop contributions to $\Delta\kappa'_V$ and ΔQ_V arising from neutral, singly, and doubly charged scalar bosons are obtained in terms of both parametric integrals and Passarino-Veltman scalar functions, which can be numerically evaluated. It is found that the GMM yields 15 (28) distinct contributions to $\Delta\kappa'_\gamma$ and ΔQ_γ ($\Delta\kappa'_Z$ and ΔQ_Z), though several of them are naturally suppressed. A numerical analysis is done in the region of parameter space still consistent with current experimental data and it is found that the largest contributions to $\Delta\kappa'_V$ arise from Feynman diagrams with two nondegenerate scalar bosons in the loop, with values of the order of $a=g^2/(96\pi^2)$ reached when there is a large splitting between the masses of these scalar bosons. As for ΔQ_V, it reaches values as large as $10^{-2}a$ for the lightest allowed scalar bosons, but it decreases rapidly as one of the masses of the scalar bosons becomes large. Among the new contributions of the GMM to the $\Delta\kappa'_V$ and ΔQ_V form factors are those induced by the $H_5^{\pm}W^{\mp}Z$ vertex, which arises at the tree level and is a unique prediction of this model.

DOI: 10.1103/PhysRevD.94.095006

I. INTRODUCTION

The observation of a 125 GeV Higgs-like particle by the CMS [1] and ATLAS [2] collaborations hints that the Higgs mechanism, responsible for mass generation of elementary particles, is realized in nature. So far, the current measurements of this particle's properties are consistent with the standard model (SM) Higgs boson. However, a more detailed and precise analysis is still necessary to confirm whether this particle is the SM Higgs boson or any other remnant scalar boson arising in an extended scalar sector from a scenario beyond the SM. In fact, from a theoretical point of view, there is no fundamental reason for a minimal Higgs sector, as occurs in the SM. It is therefore appropriate to consider additional scalar representations, which could have a role in the symmetry-breaking mechanism and establish a relationship with a yet-undiscovered sector.

Despite the great success of the SM, several extension models have been conjectured in order to solve the puzzle of some of the questions still unanswered by this theory. In this context, models with scalar triplet representations have attracted considerable attention due to their appealing features, such as the possibility of implementing the seesaw mechanism to endow the neutrinos with naturally light Majorana masses (the so-called type-II seesaw), the appearance of the $H^{\pm}W^{\mp}Z$ coupling at the tree level, and the presence of doubly charged scalar particles. In this respect, the Georgi-Machacek model (GMM) [3,4] is one of the most attractive Higgs triplet models as it preserves the relationship $\rho=1$ at the tree level via an $SU(2)$ custodial symmetry. The GMM is based mainly on the SM but in the scalar sector introduces a complex scalar triplet χ, a real scalar triplet ξ, and the usual complex scalar doublet ϕ under the $SU(2)_L\times U(1)_Y$ gauge symmetry. After the spontaneous symmetry breaking, the physical scalar spectrum of the GMM is given by the SM-like Higgs boson h and one extra CP-even singlet H; one scalar triplet H_3 ($H_3^0, H_3^{\pm}$); and one scalar fiveplet H_5 ($H_5^0, H_5^{\pm\pm}, H_5^{\pm}$). All of these multiplets are mass degenerate as a result of the custodial symmetry. The phenomenology of the GMM has been broadly studied over recent years [5–18]. For instance, a study of the search and production of the GMM Higgs bosons at the LHC has been analyzed in [16,17], and its phenomenology at a future electron-positron collider has been reported in [18].

Even if there is not enough energy available to produce the new scalar particles predicted by the GMM, one can search for their virtual effects through some observables. Particular interest has been put on the radiative corrections to the WWV ($V=\gamma, Z$) vertex, which represents a very sensitive scenario to search for any new physics (NP) effects and test the gauge sector of the SM. In fact, the one-loop corrections to the on-shell $WW\gamma$ vertex, which define the static electromagnetic properties of the W gauge boson, was one of the first ever one-loop calculations within the SM [19], followed by a plethora of calculations of the respective contributions of several SM extensions, such as the two-Higgs doublet model (THDM) [20], the minimal supersymmetric standard model (MSSM) [21], left-right symmetric theories [22], extra dimensions [23], the littlest Higgs model [24], 331 models [25,26], effective theories

[27–29], etc. In contrast with the on-shell $WW\gamma$ vertex, additional difficulties in the calculation of the on-shell WWZ vertex arise due to the nonzero mass of the Z gauge boson. In this respect, the study of radiative corrections to the WWZ vertex has been the focus of attention when the Z boson is off shell as can be found in Refs. [23,25,30,31]. These types of calculations are in general gauge dependent and require special techniques, such as the pinch technique, to extract the relevant physical information.

The on-shell WWV vertex can be written in terms of four form factors that define the CP-even and CP-odd static properties of the W boson. The two CP-odd form factors $\Delta\tilde{\kappa}'_V$ and $\Delta\tilde{Q}_V$ are absent up to the one-loop level in the SM and are thus expected to be negligibly small. As far as the CP-even form factors $\Delta\kappa'_V$ and ΔQ_V are concerned, they arise at the one-loop level in the SM and any other renormalizable theory, thereby being highly sensitive to NP effects.

The most general dimension-4 CP-conserving WWV ($V=\gamma$, Z) vertex is given by [32]

$$\mathcal{L} = -ig_V\left\{g_1^V V_\mu(W^{-\mu\nu}W_\nu^+ - W^{+\mu\nu}W_\nu^-) + \kappa_V V_{\mu\nu}W^{+\mu}W^{-\nu} + \frac{\lambda_V}{M_W^2}V^{\mu\nu}W_\nu^{+\alpha}W_{\alpha\mu}^-\right\}, \tag{1}$$

where g_V stands for the WWV tree-level coupling constant (in the SM, $g_\gamma = gs_W$ and $g_Z = gc_W$). Here g_1^V, κ_V, and λ_V represent form factors that can receive radiative corrections. In the SM, $SU(2)_L \times U(1)_Y$ gauge symmetry implies $g_1^V = \kappa_V = 1$ and $\lambda_V = 0$ at the tree level.

The vertex function that determines the WWV coupling can be written as

$$\Gamma_V^{\mu\alpha\beta} = ig_V\left\{A[2p^\mu g^{\alpha\beta} + 4(Q^\beta g^{\mu\alpha} - Q^\alpha g^{\mu\beta})] + 2\Delta\kappa'_V(Q^\beta g^{\mu\alpha} - Q^\alpha g^{\mu\beta}) + \frac{4\Delta Q_V}{m_W^2}\left(p^\mu Q^\alpha Q^\beta - \frac{1}{2}m_V^2 p^\mu g^{\alpha\beta}\right)\right\}, \tag{2}$$

where we have used the convention employed in [19] for the external momenta, as shown in Fig. 1. The form factors defined in Eq. (2) are related to those appearing in Eq. (1) according to

$$\Delta\kappa'_V \equiv \kappa_V - 1 + \lambda_V, \tag{3}$$

$$\Delta Q_V = -2\lambda_V. \tag{4}$$

It is worth mentioning that the definition $\Delta\kappa_V = \kappa_V - 1$ is customarily used in experimental works, where the constraints are given traditionally as bounds on $\Delta\kappa_V$ and λ_V, whereas in theoretical works it has been usual to present the analytical results in terms of $\Delta\kappa'_V$ and ΔQ_V.

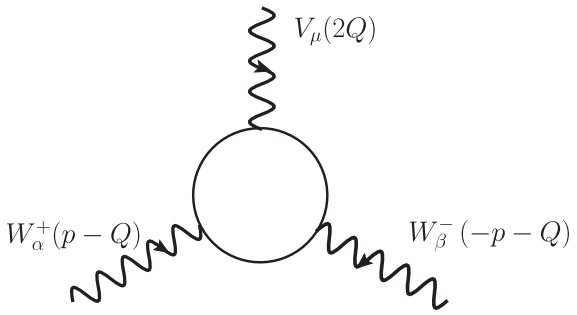

FIG. 1. Nomenclature for the WWV vertex function. The circle denotes radiative contributions.

For the photon, κ_γ and λ_γ are related to the magnetic dipole moment μ_W and the electric quadrupole moment Q_W of the W gauge boson as follows:

$$\mu_W = \frac{e}{2m_W}(1+\kappa_\gamma+\lambda_\gamma), \tag{5}$$

$$Q_W = -\frac{e}{m_W^2}(\kappa_\gamma - \lambda_\gamma). \tag{6}$$

In this work, we will calculate the contributions of the complete scalar sector of the GMM to the $\Delta\kappa'_V$ and ΔQ_V form factors, which could be at the reach of the future linear collider experiments [33,34]. The structure of our work is organized as follows. An overview of the GMM is presented in Sec. II. In Sec. III we present the analytical expressions for the $\Delta\kappa'_V$ and ΔQ form factors, whereas the numerical results are analyzed in Sec. IV and the conclusions and outlook are presented in Sec. V.

II. THE GEORGI-MACHACEK MODEL

The scalar sector of the GMM is composed by an isospin complex triplet χ with hypercharge $Y=2$, a real triplet ξ with $Y=0$, and the usual SM isospin doublet ϕ with $Y=1$. The global $SU(2)_L \times SU(2)_R$ custodial symmetry is manifest by writing the fields as

$$\Phi = \begin{pmatrix} \phi^{0*} & \phi^+ \\ -\phi^{+*} & \phi^0 \end{pmatrix}, \qquad X = \begin{pmatrix} \chi^{0*} & \xi^+ & \chi^{++} \\ -\chi^{+*} & \xi^0 & \chi^+ \\ \chi^{++*} & -\xi^{+*} & \chi^0 \end{pmatrix}, \tag{7}$$

where Φ and X transform under the custodial symmetry as $\Phi \to U_L \Phi U_R^\dagger$ and $X \to U_L X U_R^\dagger$ with $U_{L,R} = e^{i\theta_{L,R}^a T^a}$. Here $T^a = t^a$ stands for the $SU(2)$ generators in the triplet representation,

$$t^1=\frac{1}{\sqrt{2}}\begin{pmatrix}0&1&0\\1&0&1\\0&1&0\end{pmatrix},$$
$$t^2=\frac{1}{\sqrt{2}}\begin{pmatrix}0&-i&0\\i&0&-i\\0&i&0\end{pmatrix},$$
$$t^3=\frac{1}{\sqrt{2}}\begin{pmatrix}1&0&0\\0&0&0\\0&0&-1\end{pmatrix}, \tag{8}$$

whereas for the doublet representation $T^a=\sigma^a/2$, with σ^a the Pauli matrices.

The neutral members of the fields in Eq. (7) develop a nonzero vacuum expectation value (VEV) defined by $\langle\Phi\rangle=\frac{v_\phi}{\sqrt{2}}I_{2\times2}$ and $\langle X\rangle=v_\chi I_{3\times3}$, with $I_{n\times n}$ the $n\times n$ identity matrix. The masses of the W and Z gauge bosons constrain the VEVs as follows:

$$v_\phi^2+8v_\chi^2\equiv v^2=\frac{1}{\sqrt{2}G_F}\approx(246\ \text{GeV})^2. \tag{9}$$

The kinetic Lagrangian of the scalar sector, out of which the gauge boson masses arise, takes the form

$$\mathcal{L}=\frac{1}{2}\text{Tr}[(D_\mu\Phi)^\dagger(D^\mu\Phi)]+\frac{1}{2}\text{Tr}[(D_\mu X)^\dagger(D^\mu X)], \tag{10}$$

with the covariant derivative given by

$$D_\mu\Phi=\partial_\mu\Phi+i\frac{g}{2}\tau^aW_\mu^a\Phi-i\frac{g'}{2}\tau_3B_\mu\Phi, \tag{11}$$

and a similar expression for $D_\mu X$. As for the most general scalar potential that obeys the custodial symmetry, it can be written as

$$\begin{aligned}V(\Phi,X)=&\frac{\mu_2^2}{2}\text{Tr}(\Phi^\dagger\Phi)+\frac{\mu_3^2}{2}\text{Tr}(X^\dagger X)+\lambda_1[\text{Tr}(\Phi^\dagger\Phi)]^2\\&+\lambda_2\text{Tr}(\Phi^\dagger\Phi)\text{Tr}(X^\dagger X)+\lambda_3\text{Tr}(X^\dagger XX^\dagger X)\\&+\lambda_4[\text{Tr}(X^\dagger X)]^2-\lambda_5\text{Tr}(\Phi^\dagger\tau^a\Phi\tau^b)\text{Tr}(X^\dagger t^aXt^b)\\&-M_1\text{Tr}(\Phi^\dagger\tau^a\Phi\tau^b)(UXU^\dagger)_{ab}\\&-M_2\text{Tr}(X^\dagger t^aXt^b)(UXU^\dagger)_{ab},\end{aligned} \tag{12}$$

where the matrix U, which rotates X into the Cartesian basis, is given by

$$U=\begin{pmatrix}-\frac{1}{\sqrt{2}}&0&\frac{1}{\sqrt{2}}\\-\frac{i}{\sqrt{2}}&0&-\frac{i}{\sqrt{2}}\\0&1&0\end{pmatrix}. \tag{13}$$

In order to obtain the physical scalar spectrum after the spontaneous symmetry breaking, it is appropriate to decompose the neutral fields into the real and imaginary parts in the following way

$$\begin{aligned}\phi^0&\to\frac{v_\phi}{\sqrt{2}}+\frac{\phi^{0,r}+i\phi^{0,i}}{\sqrt{2}},\\\chi^0&\to v_\chi+\frac{\chi^{0,r}+i\chi^{0,i}}{\sqrt{2}},\\\xi^0&\to v_\chi+\xi^0.\end{aligned} \tag{14}$$

The physical fields are organized by their transformation properties under the $SU(2)$ custodial symmetry into a fiveplet, a triplet, and two singlets. The fiveplet and triplet states are given by

$$\begin{aligned}H_5^{++}&=\chi^{++},\qquad H_5^{+}=\frac{1}{\sqrt{2}}(\chi^+-\xi^+),\\H_5^0&=-\sqrt{\frac{2}{3}}\xi^0+\sqrt{\frac{1}{3}}\chi^{0,r},\end{aligned} \tag{15}$$

$$\begin{aligned}H_3^+&=-s_H\phi^++\frac{c_H}{\sqrt{2}}(\chi^++\xi^+),\\H_3^0&=-s_H\phi^{0,i}+c_H\chi^{0,i},\end{aligned} \tag{16}$$

where the mix between v_ϕ and v_χ is parametrized in terms of a mixing angle θ_H according to

$$c_H\equiv\cos\theta_H=\frac{v_\phi}{v},\qquad s_H\equiv\sin\theta_H=\frac{2\sqrt{2}v_\chi}{v}. \tag{17}$$

The two singlet mass eigenstates are given by

$$h=\cos\alpha\phi^{0,r}-\sin\alpha H_1^{0'},\qquad H=\sin\alpha\phi^{0,r}+\cos\alpha H_1^{0'}, \tag{18}$$

where $H_1^{0'}=\sqrt{\frac{1}{3}}\xi^0+\sqrt{\frac{2}{3}}\chi^{0,r}$, whereas h is associated with the SM Higgs boson. The mixing angle α is given by

$$\sin2\alpha=\frac{2\mathcal{M}_{12}^2}{m_H^2-m_h^2}, \tag{19}$$

with

$$\mathcal{M}_{12}^2 = \frac{\sqrt{3}}{2} v_\phi [-M_1 + 4(2\lambda_2 - \lambda_5) v_\chi]. \tag{20}$$

A peculiarity of this model is that the H_5 states are fermiophobic, which stems from the fact that there is no doublet field in the custodial fiveplet. As far as the masses of the fiveplet and triplet are concerned, they are degenerate at the tree level and are expressed in terms of the respective VEVs and the parameters involved in the scalar potential as follows:

$$m_5^2 = \frac{M_1}{4v_\chi} v_\phi^2 + 12 M_2 v_\chi + \frac{3}{2}\lambda_5 v_\phi^2 + 8\lambda_3 v_\chi^2, \tag{21}$$

$$m_3^2 = \frac{M_1}{4v_\chi}(v_\phi^2 + 8v_\chi^2) + \frac{\lambda_5}{2}(v_\phi^2 + 8v_\chi^2) = \left(\frac{M_1}{4v_\chi} + \frac{\lambda_5}{2}\right) v^2. \tag{22}$$

On the other hand, the singlet masses are given by

$$m_{h,H}^2 = \frac{1}{2}[\mathcal{M}_{11}^2 + \mathcal{M}_{22}^2 \mp \sqrt{(\mathcal{M}_{11}^2 - \mathcal{M}_{22}^2)^2 + 4(\mathcal{M}_{12}^2)^2}], \tag{23}$$

with

$$\mathcal{M}_{11}^2 = 8\lambda_1 v_\phi^2, \tag{24}$$

and

$$\mathcal{M}_{22}^2 = \frac{M_1 v_\phi^2}{4v_\chi} - 6M_2 v_\chi + 8(\lambda_3 + 3\lambda_4) v_\chi^2. \tag{25}$$

From the kinetic Lagrangian (10) one can also obtain the interactions between the SM gauge bosons and all the new scalar bosons predicted by the GMM. The full set of Feynman rules can be found in Refs. [4,15]. As far as our calculation is concerned, apart from the usual SM vertex of the type W^-W^+V ($V = \gamma$, Z), in the GMM the following new types of vertices can arise, $\phi_A^\mp \phi_A^\pm V$, $\phi_A^{\mp\mp}\phi_A^{\pm\pm}V$, $\phi_A^\mp \phi_B^{\pm\pm} W^\mp$, $\phi_A^\mp \phi_B^0 W^\pm$, $\phi_A^\mp \tilde{\phi}_B^0 W^\pm$, and $W^\mp W^\mp \phi_A^{\pm\pm}$, where $\phi_I^0 = h,\ H,\ H_5^0,\ \tilde{\phi}_I^0 = H_3^0,\ \phi_I^\mp = H_3^\mp,\ H_5^\mp$, and $\phi_I^{\mp\mp} = H_5^{\mp\mp}$ ($I = A, B$). In addition, the Z gauge boson has extra couplings of the form $\phi_A^\mp W^\pm Z$, $\phi_A^\mp \phi_B^\pm Z$, $\phi_A^0 ZZ$, and $\phi_A^0 \tilde{\phi}_B^0 Z$. It turns out that all these vertices are just of three distinct types, namely, $X_A X_A V$ (three gauge bosons), $\phi_A \phi_B X_C$ (two scalar bosons and one gauge boson), and $\phi_A X_B X_C$ (one scalar boson and two gauge bosons), where ϕ_I ($I = A, B$) stands for a neutral, singly charged or doubly charged scalar boson, whereas X_J ($J = A, B, C$) stands for a neutral or charged gauge boson. Evidently, the allowed vertices are dictated by electric charge conservation, Bose symmetry, CP invariance (as long as it is assumed to be conserved), etc. However, the Lorentz structure is similar for each type of vertex and so are the respective Feynman rules, which arise from the following Lagrangians:

$$\mathcal{L}_{X_A X_A V} = i g_{X_A X_A V}(X_{A\mu\nu}^\dagger V^{\mu\nu} - X_A^{\mu\nu} X_{A\mu}^\dagger V_\nu + V^{\mu\nu} X_{A\mu}^\dagger X_{A\nu}), \tag{26}$$

$$\mathcal{L}_{\phi_A \phi_B X_C} = i g_{\phi_A \phi_B V} X_C^\mu \phi_A^\dagger \overleftrightarrow{\partial}_\mu \phi_B, \tag{27}$$

and

$$\mathcal{L}_{X_A X_B \phi_C} = g_{X_A X_B \phi_C} X_A^\mu X_{B\mu} \phi_C, \tag{28}$$

with $X_A^{\mu\nu} = \partial^\mu X_A^\nu - \partial^\nu X_A^\mu$. We have assumed that CP is conserved.

For the photon, the only allowed vertices are $WW\gamma$, $\phi^\mp \phi^\pm \gamma$, and $\phi^{\mp\mp}\phi^{\pm\pm}\gamma$, whereas the Z gauge boson can also have nondiagonal couplings to both charged and neutral scalar bosons. From Eqs. (26)–(28), generic Feynman rules follow straightforwardly and are shown in Fig. 2. Therefore, we can perform a model-independent calculation and express our results in terms of the coupling constants and the masses of the virtual particles. In

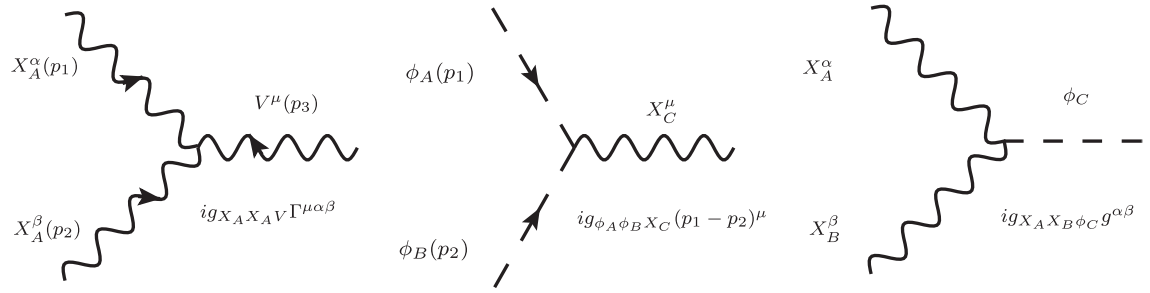

FIG. 2. Generic Feynman rules for the relevant vertices involved in our calculation. The arrows stand for the direction of the 4-momenta and $\Gamma_{\mu\alpha\beta} = g_{\mu\alpha}(p_1 - p_3)_\beta + g_{\alpha\beta}(p_2 - p_1)_\mu + g_{\beta\mu}(p_3 - p_2)_\alpha$. $V = \gamma, Z$, ϕ_I ($I = A, B, C$) denote a neutral singly or doubly charged scalar boson, and X_J ($J = A, B$) stands for a neutral or charged gauge boson. The electric charge and CP properties of the particles attached to each vertex are dictated by electric charge conservation, Bose symmetry, CP invariance, etc.

particular, the coupling constants for the vertices allowed in the GMM are presented in Appendix A.

III. $\Delta\kappa_V'$ AND ΔQ_V FORM FACTORS IN THE GMM

We now turn to present the contributions of the scalar sector of the GMM to the $\Delta\kappa_V'$ and ΔQ_V form factors at the one-loop level. In this model, the new one-loop contributions arise from generic triangle diagrams (the bubble diagrams do not contribute) that can be classified according to the number of distinct particles circulating into the loop. In Fig. 3 we show a set of Feynman diagrams that contribute to both the $WW\gamma$ and WWZ vertices. These diagrams include just two distinct particles circulating inside the loop as they involve diagonal couplings of the form $\phi_A\phi_A V$ and $X_A X_A V$.

Contrary to the couplings of the photon to a pair of charged scalar bosons, which can only be of diagonal type due to electromagnetic gauge invariance, the Z gauge boson can have nondiagonal couplings to a pair of neutral or charged scalar bosons. Therefore, in addition to the diagrams of Fig. 3, the $\Delta\kappa_Z'$ and ΔQ_Z form factors can receive extra contributions from the Feynman diagrams shown in Fig. 4, which have three distinct particles circulating into the loop. Below we will present the contributions to $\Delta\kappa_V'$ and ΔQ_V for all these types of diagrams.

Before presenting our results, some remarks about our calculation are in order:

(i) The Feynman diagrams were evaluated via the unitary gauge. In order to make a cross-check of our results we used both the Feynman parametrization technique and the Passarino-Veltman method to solve the loop integrals.

(ii) We verified that all the contributions of bubble diagrams to the $\Delta\kappa_V'$ and ΔQ_V form factors involving quartic vertices with two scalar bosons and two gauge bosons vanish, and thus the only contributions arise from triangle diagrams.

(iii) The mass shell and transversality conditions for the gauge bosons enabled us to make the following replacements,

$$Q^2 = \frac{m_V^2}{4}, \qquad p\cdot Q = 0, \qquad p^2 = m_W^2 - \frac{m_V^2}{4}, \tag{29}$$

and

$$p_\alpha \to Q_\alpha, \qquad p_\beta \to -Q_\beta, \qquad p_\mu \to 0, \tag{30}$$

which results in a considerable simplification of the calculation.

(iv) Instead of dealing with the calculation of the $WW\gamma$ and WWZ vertices separately, we performed the calculation of the general WWV vertex, with V a massive neutral gauge boson. We have exploited the fact that there are only three generic trilinear vertices involved in the one-loop contributions to the WWV vertex and thus a model-independent calculation was done using the generic Feynman rules of Fig. 2. The result for the contribution of each type of Feynman diagram will be presented in terms of loop functions, given as parametric integrals and also in terms of Passarino-Veltman scalar integrals, times a factor involving all the generic coupling constants associated with each vertex participating in the particular diagram. The contributions to the form factors of the $WW\gamma$ and WWZ vertices follow easily from our general expressions after taking the appropriate mass limits and substituting the corresponding coupling constants of the GMM or any other extension model.

(v) We corroborated that the WWV amplitude arising from each type of diagram can be cast in the form of Eq. (2) and also that all the contributions to the $\Delta\kappa_V'$ and ΔQ_V form factors are free of ultraviolet divergences.

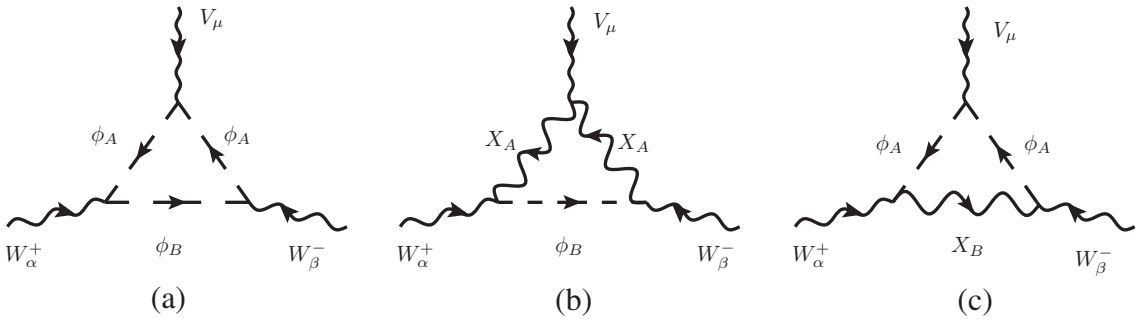

FIG. 3. Generic Feynman diagrams for the new scalar contributions to both the $WW\gamma$ and WWZ vertices involving only two distinct virtual particles. The arrows stand for the directions of the 4-momenta. The possible combinations of internal particles are given by the vertices allowed in each particular model. For instance, when $V = \gamma$, the following electric charges of the internal particles are possible in the GMM, in units of the positron charge: if $Q_A = -1$ then $Q_B = 0$, if $Q_A = 1$ then $Q_B = 2$, and if $Q_A = -2$ then $Q_B = -1$.

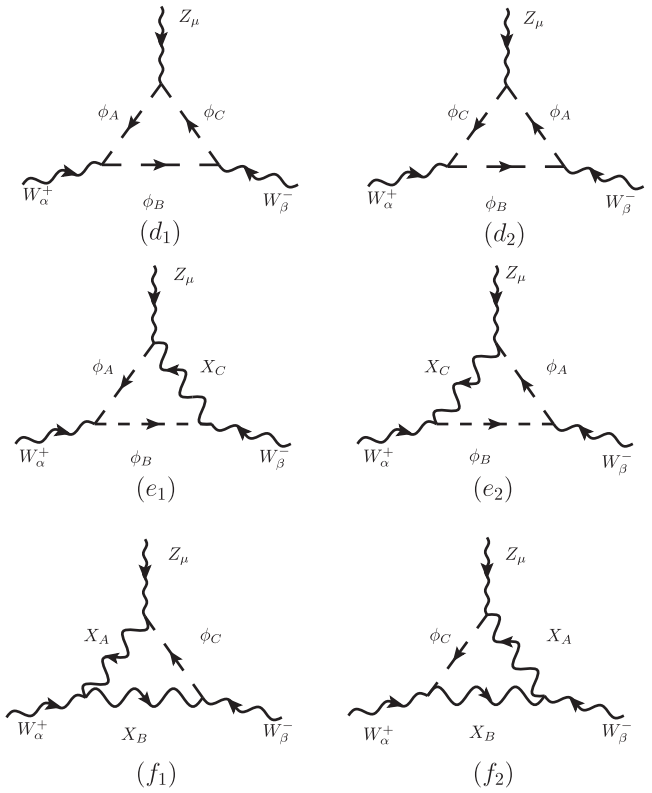

FIG. 4. Extra contributions to the $\Delta\kappa'_Z$ and ΔQ_Z form factors from nondiagonal couplings. As explained in the text, the possible sets of internal particles are determined by the vertices allowed in a particular model.

We now proceed to present the results. Once the amplitude for each Feynman diagram is written down with the help of the Feynman rules of Fig. 2, the Feynman parametrization technique and the Passarino-Veltman method can be applied straightforwardly, followed by some lengthy algebra. Thereafter one can express the contributions to the $\Delta\kappa'_V$ and ΔQ_V form factors for each type of Feynman diagram of Fig. 3 as follows:

$$\Delta\kappa'^i_V = -\frac{C^i_V}{16\pi^2} I^{V-i}_\kappa(x_A, x_B, x_V), \tag{31}$$

$$\Delta Q^i_V = -\frac{C^i_V}{16\pi^2} I^{V-i}_Q(x_A, x_B, x_V), \tag{32}$$

for $V = Z, \gamma$ and $i = a, b, c$. We have introduced the scaled variable $x_I = m_I^2/m_W^2$ ($I = A, B$), with m_A and m_B denoting the masses of the particles circulating into each type of diagram. A word of caution is in order here as m_A and m_B, and thereby x_A and x_B, are distinct for each type of contribution. As for the loop functions I^{V-i}_κ and I^{V-i}_Q, they are presented in Appendix B in terms of parametric integrals and Passarino-Veltman scalar integrals, together with the explicit form of the C^i_V factors, which are given in terms of the coupling constants of the vertices involved in each Feynman diagram. These coefficients are presented in Appendix C for each possible contribution arising in the GMM.

As explained above, the $\Delta\kappa'^i_\gamma$ and ΔQ^i_γ form factors can be obtained from the general expressions (31)–(32), and the loop functions presented in Appendix B, by taking the $m_V \to 0$ limit. The resulting loop functions $I^{\gamma-i}_{\kappa,Q}$ are also shown in this Appendix. We have verified that these expressions are in agreement with the results presented in Ref. [24], where the $WW\gamma$ vertex was studied in the context of little Higgs models.

As far as the Feynman diagrams of Fig. 4 are concerned, they only contribute to the WWZ vertex and the respective form factors depend now on three distinct internal masses. They can be written as follows:

$$\Delta\kappa'^i_Z = -\frac{C^i_Z}{16\pi^2} I^{Z-i}_\kappa(x_A, x_B, x_C, x_Z), \tag{33}$$

$$\Delta Q^i_Z = -\frac{C^i_Z}{16\pi^2} I^{Z-i}_Q(x_A, x_B, x_C, x_Z). \tag{34}$$

This time the superscript i stands for the total contributions of diagrams i_1 and i_2, with $i = d, e, f$. Expressions for the loop functions in terms of both parametric integrals and Passarino-Veltman scalar integrals can be found in Appendix B.

Once the general expressions for the different kinds of contributions are obtained, we can compute the total contribution of the scalar sector of a given model by simply adding up all the partial contributions. We will present below a numerical analysis of the contributions of the GMM. For the numerical evaluation we computed the parametric integrals via the Mathematica numerical routines. A cross-check was done via the numerical evaluation of the results given in terms of Passarino-Veltman scalar functions [35] with the help of the LoopTools routines [36,37].

IV. NUMERICAL DISCUSSION

In order to make a numerical evaluation of the contribution of the GMM to the $\Delta\kappa'_V$ and ΔQ_V form factors, it is necessary to take into account the current constraints on the parameter space of this model. In particular, our results depend on five free parameters, namely, the singlet mixing angle α, the mixing angle between the doublet and the triplet θ_H, and the masses of the new singlet m_H, the triplet m_{H_3}, and the fiveplet m_{H_5}. A recent study on the indirect constraints on the GMM from B physics and electroweak precision observables can be found in [38], where the limit on the triplet VEV $v_\chi \leq 65$ GeV, arising from the measurement of the $b \to s\gamma$ process, was used to impose the strongest bound $\sin\theta_H \leq 0.75$. On the other hand, the current LHC measurements of the couplings and signal

strength of the SM-like Higgs boson production [39,40] constrain in a direct way the $\theta_H - \alpha$ plane [17]. As for the masses of the new scalar bosons, experimental constraints on the fiveplet mass have been derived by the ATLAS Collaboration using the like-sign $WWjj$ production cross-section measurement [41]. Furthermore, theoretical constraints from unitarity and vacuum electroweak stability limit the mass of all the scalar bosons of the GMM to be less than 1 TeV [14,15,42,43]. This constraint was obtained assuming a Z_2 symmetry obeyed by the scalar potential in order to reduce the number of free parameters. However, a study presented in Ref. [14] showed that when the most general potential (14) is considered, there is a decoupling limit in which the masses of the new scalar bosons can be heavy. Therefore, it is interesting considering the scenario when the masses of the new scalar bosons can be heavier than 1 TeV.

A. $\Delta\kappa'_\gamma$ and ΔQ_γ form factors

We list in Tables III–V of Appendix C all the contributions of the GMM to both $\Delta\kappa'_\gamma$ and ΔQ_γ, including the list of particles circulating into each loop and the explicit form of the corresponding C^i_γ coefficient. Excluding the pure SM contributions, the $\Delta\kappa'_\gamma$ and ΔQ_γ form factors receive ten contributions of the type-(a) diagrams, three of the type-(b) diagrams, and two of the type-(c) diagrams. Notice that all the new scalar bosons participate in the type-(a) diagrams, whereas the type-(b) diagrams only receive contributions from the singlet and the fiveplet scalar bosons, and the type-(c) diagrams from the fiveplet scalar bosons only. We first examine the general behavior of $\Delta\kappa'_\gamma$ and ΔQ_γ as functions of the masses of the scalar bosons. For the type-(b) and type-(c) contributions we show in Fig. 5 the form factors as a function of the mass of the scalar boson circulating into the loop, whereas for the type-(a) diagram we consider two scenarios: when both scalar bosons are degenerate and when one scalar boson mass is fixed and the other one is variable.

We first discuss the behavior of $\Delta\kappa'_\gamma$ (left plot of Fig. 5). As far as the type-(a) contribution is concerned, it depends on the masses of two scalar bosons S_1 and S_2 and is highly dependent on the splitting between their masses $\Delta m_{21} = m^2_{S_2} - m^2_{S_1}$. When such a splitting is vanishing or very small, $m_{S_2} \simeq m_{S_1}$, this contribution decreases quickly as m_{S_1} increases (dashed line), but it tends to a nonvanishing constant value when the splitting becomes large (solid line), which is in accordance with the decoupling theorem as discussed in Ref. [44]. It is worth mentioning that the sharp dip observed in the solid line is due to a change of sign of the form factor, which can become important as there could be large cancellations between contributions due to this change of sign. On the other hand, the type-(b) and type-(c) contributions only depend on one scalar boson mass and they are larger for a light scalar boson but decrease quickly when the scalar boson mass increases. It is important to notice that the $C^{b,c}_\gamma$ constants are proportional to the VEV v; thus the size of this type of contribution will increase by around two orders of magnitude with respect to the values shown in the plots. Even when the scalar boson masses are relatively light, the type-(a) contribution is the dominant one, except for degenerate masses, when all the contributions are of similar size. In summary, the dominant contribution to $\Delta\kappa'_\gamma$ is expected to arise from type-(a) diagrams, except for a possible suppression due to the C^i_γ factor and possible cancellations between distinct contributions. The largest $\Delta\kappa'_\gamma$ value is reached when the scalar boson masses m_{S_1} and m_{S_2} are relatively light or when there is a large mass splitting Δm_{12}.

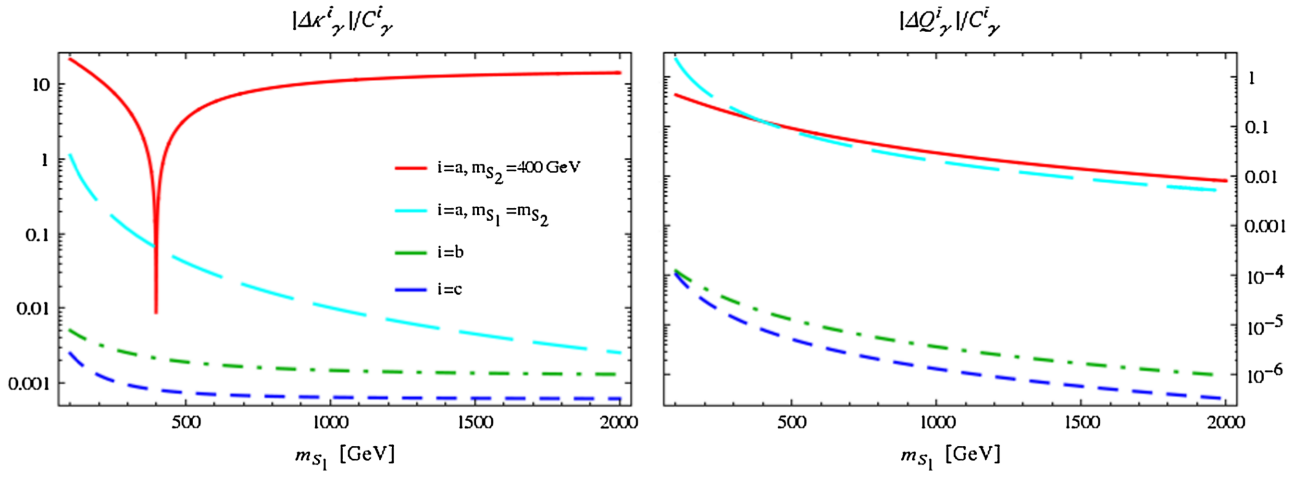

FIG. 5. Behavior of the contributions of the diagrams of Fig. 3 to the $\Delta\kappa'_\gamma$ and ΔQ_γ form factors as functions of the masses of the scalar bosons circulating into the loops of each type of contribution divided by the C^i_γ coefficient and in units of $a = g^2/(96\pi^2)$. While the type-(a) contribution depends on two scalar boson masses m_{S_1} and m_{S_2}, the type-(b) and type-(c) diagrams depend on only one scalar boson mass m_{S_1}.

We now turn to analyze the ΔQ_γ form factor, whose dependence on the scalar boson masses is shown in the right plot of Fig. 5. We observe that this form factor exhibits a different behavior to that of $\Delta\kappa'_\gamma$. Although type-(a) contributions are also larger than type-(b) and type-(c) contributions, in this case there is no dependence on the mass splitting Δm_{21} and all the contributions decrease when at least one of the scalar boson masses becomes large. However, the decrease of ΔQ_γ as m_{S_1} increases is less pronounced that in the case of $\Delta\kappa'_\gamma$. Therefore, barring an extra suppression due to the size of the C_γ^i coefficients and possible cancellations, the largest contributions to ΔQ_γ will arise from type-(a) diagrams provided that all the scalar boson masses are light. The contribution to this form factor is dominated by the heaviest scalar boson circulating in the type-(a) diagrams and will be very suppressed even if the other scalar boson is relatively light. In type-(b) and type-(c) diagrams there is also a strong suppression for a heavy scalar boson.

When adding up all the partial contributions to $\Delta\kappa'_\gamma$ and ΔQ_γ, there could be extra suppression due to the size and sign of the C_γ^i coefficients and the loop functions. For instance, s_H is constrained to be less than 10^{-1} and thus any contribution proportional to this parameter will have a suppression factor of the order of 10^{-2} and will be negligible unless the remaining contributions are also suppressed. All the contributions of this kind arise from diagrams involving a weak gauge boson and a fiveplet scalar boson. Therefore, all the type-(c) contributions and the type-(b) contributions numbers 2 and 3 (for the number of each contribution, see Tables III through VIII) will be two orders of magnitude smaller than the remaining contributions, although there is a region of the parameter space in which all the contributions are equally suppressed. Even more, the type-(b) contribution number 1 arises from the loop with the W gauge boson and the H scalar boson, being proportional to the square of the coefficient $f_H = \frac{1}{6}(3c_H s_\alpha - 2\sqrt{6}s_H c_\alpha)$, which is very small for small s_α and s_H. Therefore, in most of the allowed region of the parameter space, the largest contributions will arise from the type-(a) diagrams with two nondegenerate scalar bosons, though the diagram including the SM Higgs boson and a triplet scalar boson is considerably suppressed as the coefficient g_h^2 is very suppressed too. In addition, due to the relative change of sign between distinct contributions there could be large cancellations once all the type-(a) contributions are added up and so there could be regions of the parameter space where all three types of contributions are of similar size. However, this region is not the one in which the largest contributions to the form factors can arise.

All the properties discussed above will reflect on the general behavior of the total contribution from the GMM to the $\Delta\kappa'_\gamma$ and ΔQ_γ form factors, which we have evaluated as functions of the scalar boson masses. For the mixing angles we used two combinations of values lying inside the allowed area of the parameter space determined by the authors of Ref. [16] in their study of fiveplet state production at the LHC. We thus considered the sets of values $(s_H, s_\alpha) = (0.1, 0.2)$ and $(s_H, s_\alpha) = (0.1, -0.3)$, which allows us to illustrate the behavior of $\Delta\kappa'_\gamma$. As for the masses of the scalar bosons we fix the value of the mass of the singlet scalar m_H to either 400 GeV or 1000 GeV, and plot in Fig. 6 the contour lines of $\Delta\kappa'_\gamma$ in the m_{H_3} vs m_{H_5} plane. In all these plots the main contributions to $\Delta\kappa'_\gamma$ arise from type-(a) diagrams, though in some regions the type-(b) contributions can be of similar size. We observe that for small m_H (left plots) the largest contributions are reached for large m_{H_3} and small m_{H_5} and vice versa (lightest area). The region in which m_{H_3} and m_{H_5} are almost degenerate appears in the plots as a dark strip and is the region in which $\Delta\kappa'_\gamma$ reaches its lowest values. On the other hand, when m_H is large (right plots) we observe that $\Delta\kappa'_\gamma$ reaches its largest values for large m_{H_3} and light m_{H_5}, but in this case there is no such increase when m_{H_5} is large and m_{H_3} remains small, as there are cancellations between the distinct contributions. The dark strip where this form factor reaches its lowest values now has shifted upwards but in general encompasses the area where the three scalar boson masses are large and thereby almost degenerate, namely, the top right corners of these plots. We also observe that a change in s_α has a slight impact on the behavior of $\Delta\kappa'_\gamma$. However, irrespective of the value of s_α, in general the largest values of $\Delta\kappa'_\gamma$ correspond to the scenarios where there is a large splitting between the scalar boson masses and the smallest values correspond to the case when the three masses are large or degenerate. The largest values of $\Delta\kappa'_\gamma$, in the explored region of the parameter space, are of the order of a. In general the largest contributions arise from type-(a) contributions numbers 2, 4, 5, 7, and 9, but when all the masses of the scalar bosons are degenerate these contributions are suppressed and are of a similar size as the type-(b) contribution number 1, which in general is more suppressed than type-(a) contributions.

We now turn to the analysis of the behavior of the ΔQ_γ form factor. We consider the same scenarios as in the study of $\Delta\kappa'_\gamma$ and show in Fig. 7 the contour plot for ΔQ_γ in the m_{H_5} vs m_{H_3} plane. As discussed above, contributions of type-(a) have now no dependence on the splitting of the scalar boson masses and they decrease rapidly as at least one of the scalar boson masses becomes large. Therefore, type-(a) contributions will reach their largest values in the region (the lightest area) where the masses of both scalars running into the loop are relatively light. As for the type-(b) contributions, they have a similar behavior to type-(a) contributions as they decrease as the scalar boson mass increases, though in general they are smaller than type-(a) contributions and so are type-(c) contributions. The behavior of the total contribution to ΔQ_γ will thus be dominated by the type-(a) contributions and will be larger for light degenerate scalar boson masses. This is illustrated in the four plots of Fig. 7 in

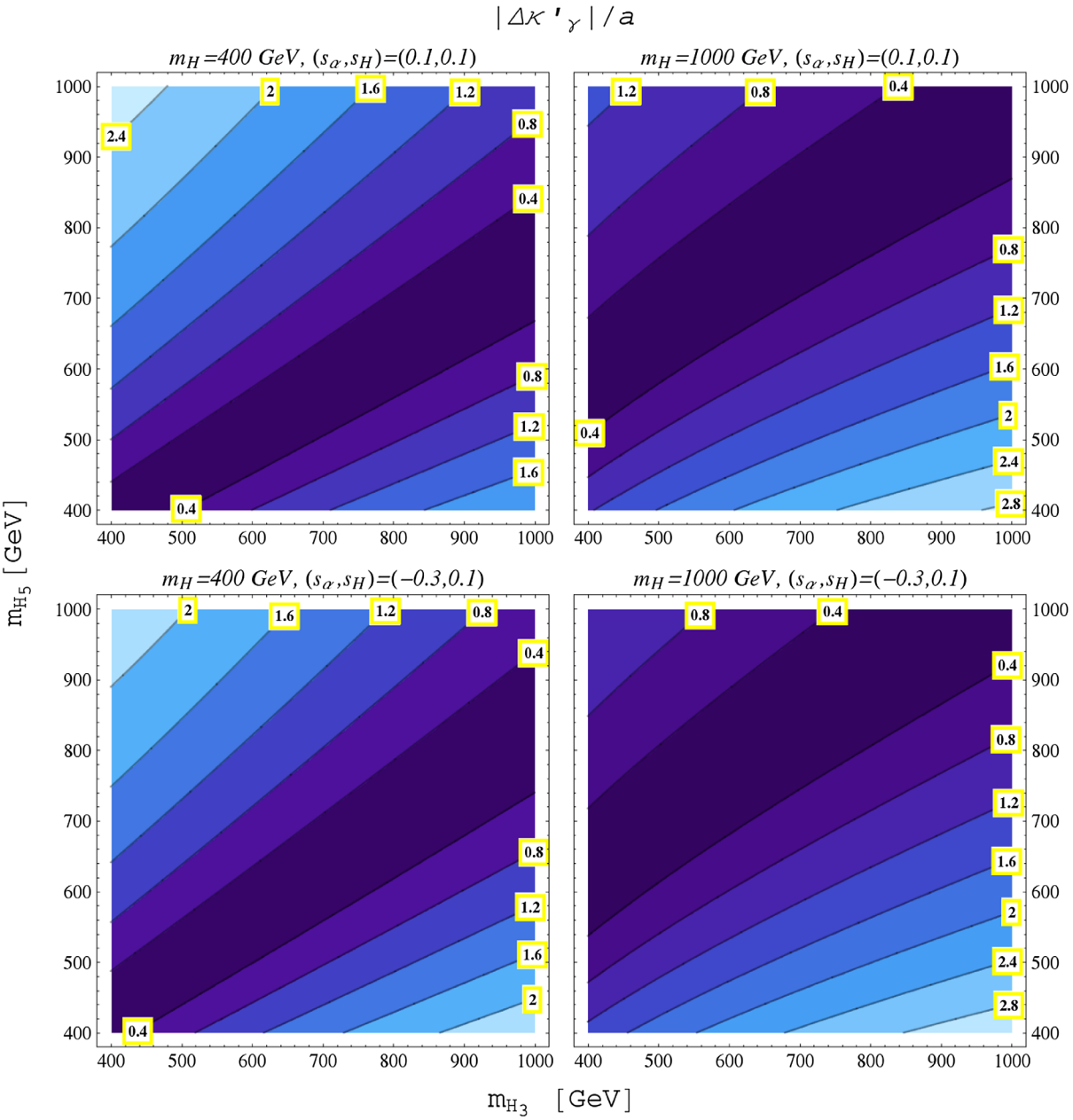

FIG. 6. Contour plot for the $\Delta\kappa'_\gamma$ form factor in the GMM in the m_{H_3} vs m_{H_5} plane for a fixed value of m_H and the indicated values of the mixing angles s_H and s_α.

which the largest contributions are reached for small degenerate masses and they decrease when either m_{H_3} or m_{H_5} becomes large, though this decrease remains smooth up to masses of about 800 GeV. In this case the dominant contributions arise from the type-(a) contributions numbers 6, 8, and 10. When all the masses of the scalar bosons are light, the type-(a) contribution number 2 is of a similar size as contributions 6, 8, and 10, whereas all other contributions are suppressed due to the small value of the corresponding coefficient C_γ^a. In general, the largest values reached by ΔQ_γ are of the order of 1% of a and there is a slight dependence on the value of s_α.

It is interesting to note that the contributions of the GMM to $\Delta\kappa'_\gamma$ are about two orders of magnitude larger than those to ΔQ_γ. Such a behavior of the $WW\gamma$ form factors, which was also observed for instance in the context of a model with technihadrons [45] and the minimal 331 model [44], can be explained in the light of the decoupling theorem. It turns out that $\Delta\kappa'_\gamma$ and ΔQ_γ appear in the $WW\gamma$ vertex function (2) as coefficients of Lorentz structures of canonical dimension 4 and 6, respectively. This means that $\Delta\kappa'_\gamma$ can be sensitive to nondecoupling effects of heavy particles, whereas ΔQ_γ is always insensitive to such effects and a natural suppression of this form factor by inverse

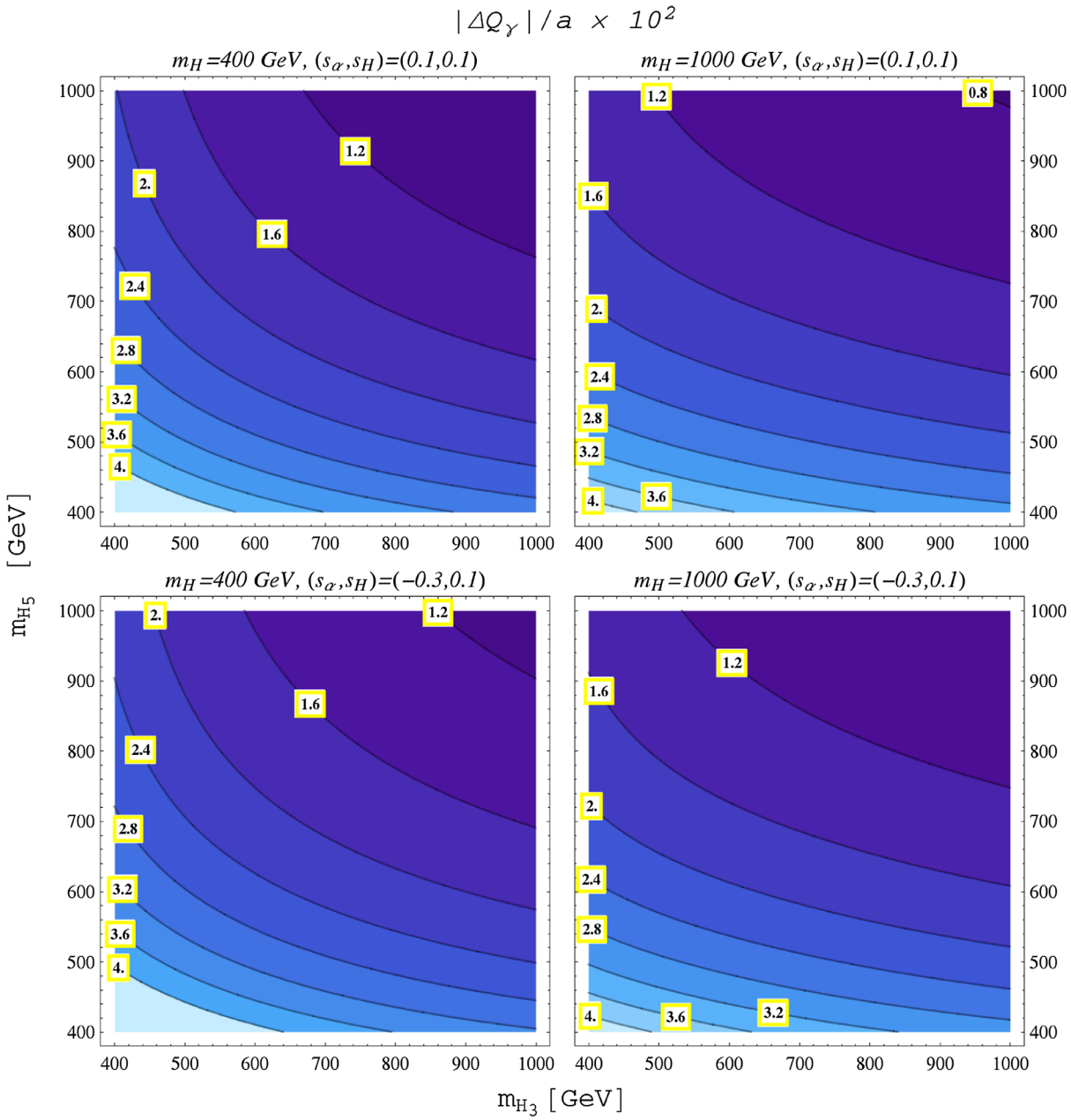

FIG. 7. The same as in Fig. 6, but for the ΔQ_γ form factor.

powers of the mass of the heaviest particle inside the loop is expected. In the present analysis we have considered the contributions of heavy scalar bosons, which explains the observed behavior of the $WW\gamma$ form factors. For a more general discussion of this issue we refer the interested reader to Refs. [44–46]. We will see below that, as expected, this feature is also present in the behavior of the $\Delta\kappa_Z'$ and ΔQ_Z form factors.

B. $\Delta\kappa_Z'$ and ΔQ_Z form factors

We will now analyze the $\Delta\kappa_Z'$ and ΔQ_Z form factors, for which we will follow a similar approach to that used above. We thus start by studying the general behavior of the distinct types of contributions. Apart from the diagrams of Fig. 3, there are additional contributions due to the diagrams of Fig. 4. As for the contributions of types (a), (b), and (c), their behavior is quite similar to that observed in Fig. 5, so we will focus on the analysis of the extra contributions, whose behavior will turn out to be rather similar to that of contributions of type (a), (b), and (c), respectively. As shown in Appendix C, in the GMM there are seven contributions of type (d), four of type (e), and three of type (f). Although our general results allow us to calculate type-(d) contributions with three distinct scalar boson masses m_{S_1}, m_{S_2}, and m_{S_3}, in the GMM all the masses of the same

multiplet are degenerate. It means that type-(d) contributions arise only from diagrams with at least two degenerate scalar bosons. Also, although type-(e) contributions arise from diagrams that can have two distinct scalar bosons, their masses are degenerate and there is dependence on one mass only, and this is also true for type-(f) contributions. Therefore, we expect that type-(d) contributions will be the dominant contribution to $\Delta\kappa'_Z$ as long as there is a large splitting between the scalar boson masses, whereas type-(e) and type-(f) contributions will only be important for a relatively light scalar boson mass. This is depicted in Fig. 8, where we show the behavior of the $\Delta\kappa'_Z$ and ΔQ_Z form factors for all the scenarios allowed in the GMM. For type-(d) contributions we consider three scenarios: m_{S_3} fixed and $m_{S_2} = m_{S_1}$ variables, $m_{S_3} = m_{S_2}$ fixed and m_{S_1} variable, and the three scalar boson masses degenerate $m_{S_3} = m_{S_2} = m_{S_1}$. On the other hand, for type-(e) contributions we only consider the case when the two scalar bosons are degenerate. In Fig. 8 we observe that $\Delta\kappa'_Z$ and ΔQ_Z have a similar behavior to that of the $\Delta\kappa'_\gamma$ and ΔQ_γ form factors. In particular, the largest contributions to $\Delta\kappa'_Z$ are reached when there is a large splitting between the scalar masses or when all the scalar boson masses circulating into each loop are relatively light. However, the decrease of $\Delta\kappa'_Z$ for large m_{S_1} is now less quick than in the case of $\Delta\kappa'_\gamma$. Again, the C^i_Z factor is proportional to v for type-(e) and type-(f) contributions, so the values shown in the plots will increase by two orders of magnitude for these contributions. As for ΔQ_Z, it will reach its largest value for the smallest allowed scalar boson masses as in the case of ΔQ_γ. When the scalar bosons are very heavy, they will be approximately degenerate, in which case ΔQ_Z will decrease significantly. Extra suppression for both form factors can arise from the C^i_Z coefficients and from potential cancellations between the distinct contributions as in the case of the electromagnetic form factors.

In Fig. 9 we present the contour plots for $\Delta\kappa'_Z$ for the same sets of parameter values used above. In spite of the extra contributions, the behavior of this form factor is rather similar to that of $\Delta\kappa'_\gamma$. We first note that all the contributions of types (c), (e), and (f) have an extra suppression due to the s^2_H factor appearing in the respective C^i_Z coefficient and thus the main contributions will arise from type-(a) and type-(d) contributions, and to a lesser extent from type-(b) contribution number 1. All other contributions are only important in regions of the parameter space where the dominant contributions are suppressed by the respective loop function. As far as the scenario with $s_\alpha = 0.1$ is concerned, we observe in the top left plot, in which we use $m_H = 400$ GeV, that the largest contributions arise when either m_{H_3} or m_{H_5} is large, whereas in the top right plot we observe that there is enhancement only when m_{H_3} is large and m_{H_5} remains small, but not in the opposite case. It means that there are cancellations between contributions when m_{H_5} and m_H are large and thus the total contribution does not increase in spite of the large splitting between m_{H_5} and m_{H_3}. When the three masses m_H, m_{H_3}, and m_{H_5} are degenerate the total contribution is suppressed by about one order of magnitude. Even if all the scalar boson masses are relatively light, $\Delta\kappa'_Z$ is smaller than in the case where either m_{H_3} or m_{H_5} is large. In the bottom plots we use $s_\alpha = -0.3$ and observe that the behavior of $\Delta\kappa'_Z$ has a slight change due to the change in the values of the C^i_Z coefficients; however its largest values are also of the order of a. The darkest strip where $\Delta\kappa'_Z$ reaches its smallest values, which corresponds to nearly degenerate m_{H_3} and m_{H_5}, has now shifted downwards. In summary, the largest values of $\Delta\kappa'_Z$, in this region of the parameter space, are of the order of a, and are reached when there is a large splitting between the masses' scalar bosons. In general the largest contributions to $\Delta\kappa'_Z$ arise from type-(a) and type-(d) diagrams, with the

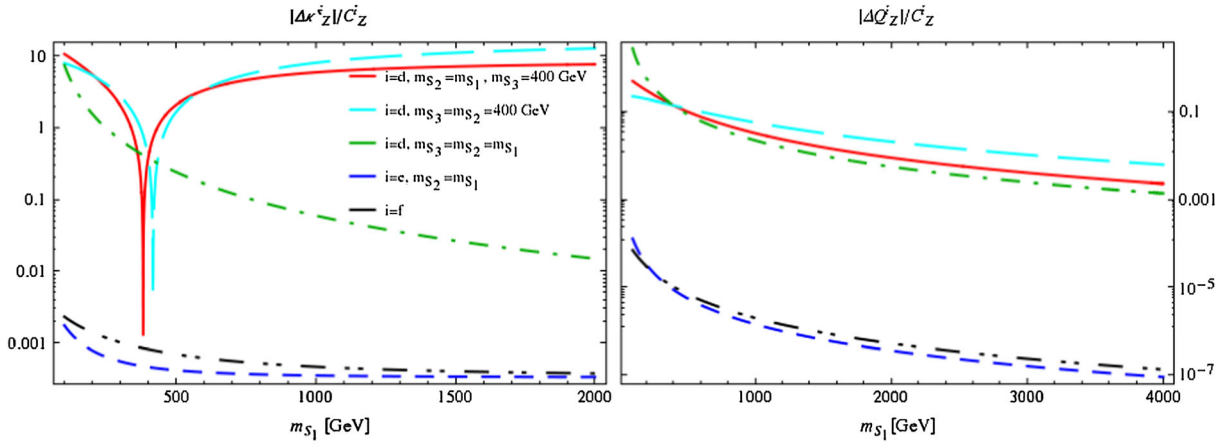

FIG. 8. Behavior of the contribution of diagrams of Fig. 4 to the $\Delta\kappa'_Z$ and ΔQ_Z form factors as a function of the masses of the scalar bosons circulating into the loops of each type of contribution divided by the C^i_Z coefficient and in units of a. Type-(d) contribution depends on three scalar boson masses m_{S_1}, m_{S_2}, and m_{S_3}; type-(e) depends on two scalar masses m_{S_1} and m_{S_2}; and type-(f) diagrams depend on only one scalar boson mass m_{S_1}. We only consider the possible scenarios arising in the GMM.

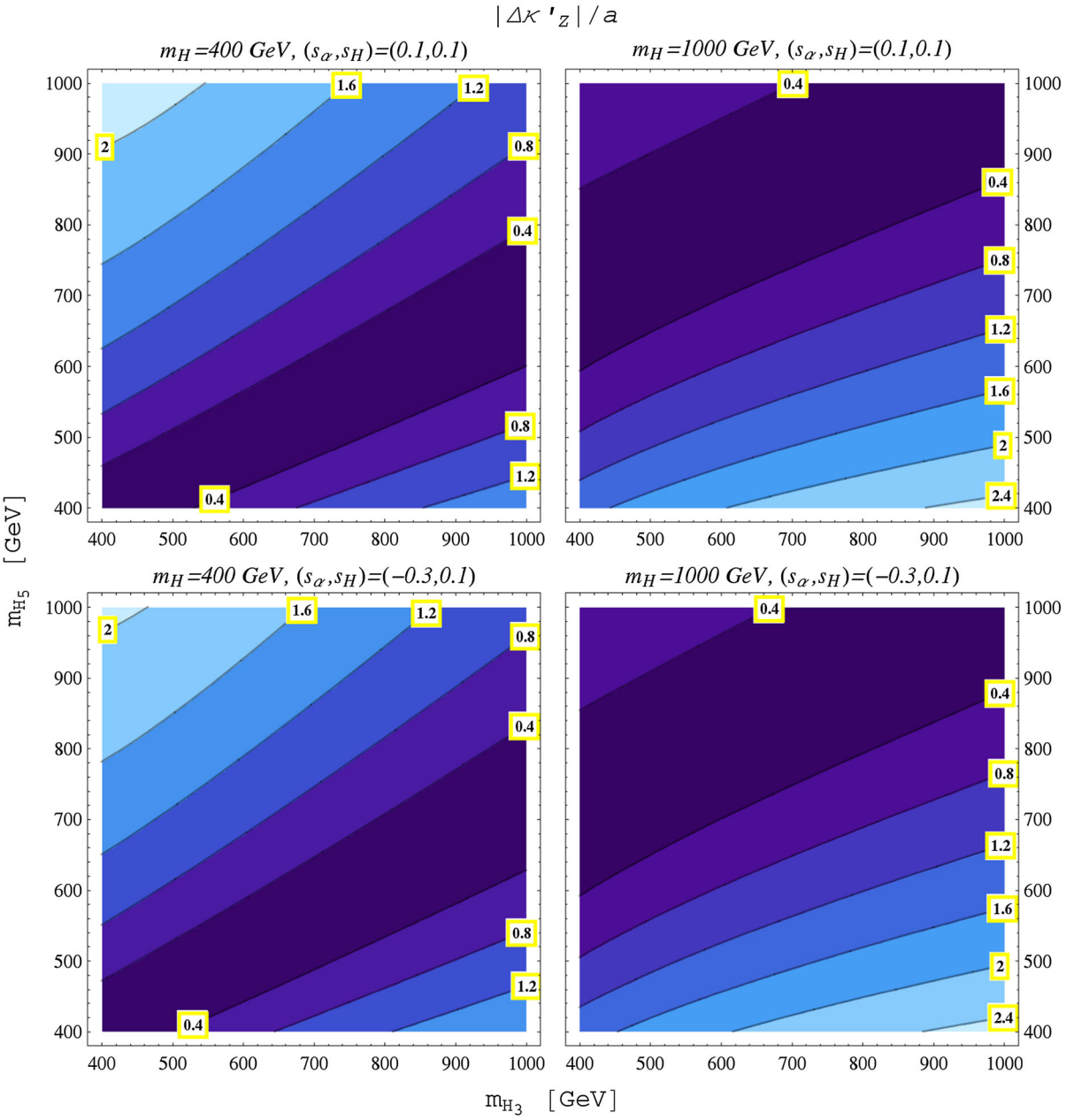

FIG. 9. Contour plot for the $\Delta\kappa_Z'$ form factor in the GMM in the m_{H_3} vs m_{H_5} plane for a fixed value of m_H and the indicated values of the mixing angles s_H and s_α.

type (b), (e), and (f) diagrams yielding a subdominant contribution, which is only relevant when all the masses of the scalar bosons are degenerate.

We now turn to the analysis of the behavior of the ΔQ_Z form factor, which is shown in Fig. 10 in the m_{H_5} vs m_{H_3} plane. As discussed above, in this case there is no enhancement due to a large splitting of the scalar boson masses but a decrease when at least one of the masses of the scalar bosons becomes large. Therefore, contributions of types (a) and (d) reach their largest values provided that all the scalar boson masses are relatively light. As for the remaining contributions, they have a similar behavior as they decrease as the scalar boson mass increases, though in general they are smaller than type-(a) and type-(d) contributions. We observe that the largest contributions to ΔQ_Z arise from diagrams including only fiveplet scalar bosons provided that m_{H_5} is relatively light irrespective of the value of m_H and m_{H_3}. The behavior of the total contribution to ΔQ_Z is thus dominated by type-(a) contributions numbers 6, 8, and 10, reaching its largest values for light m_{H_5}. Note that type-(a) contributions are the only ones that can involve fiveplet scalar bosons only. When all the masses of the scalar

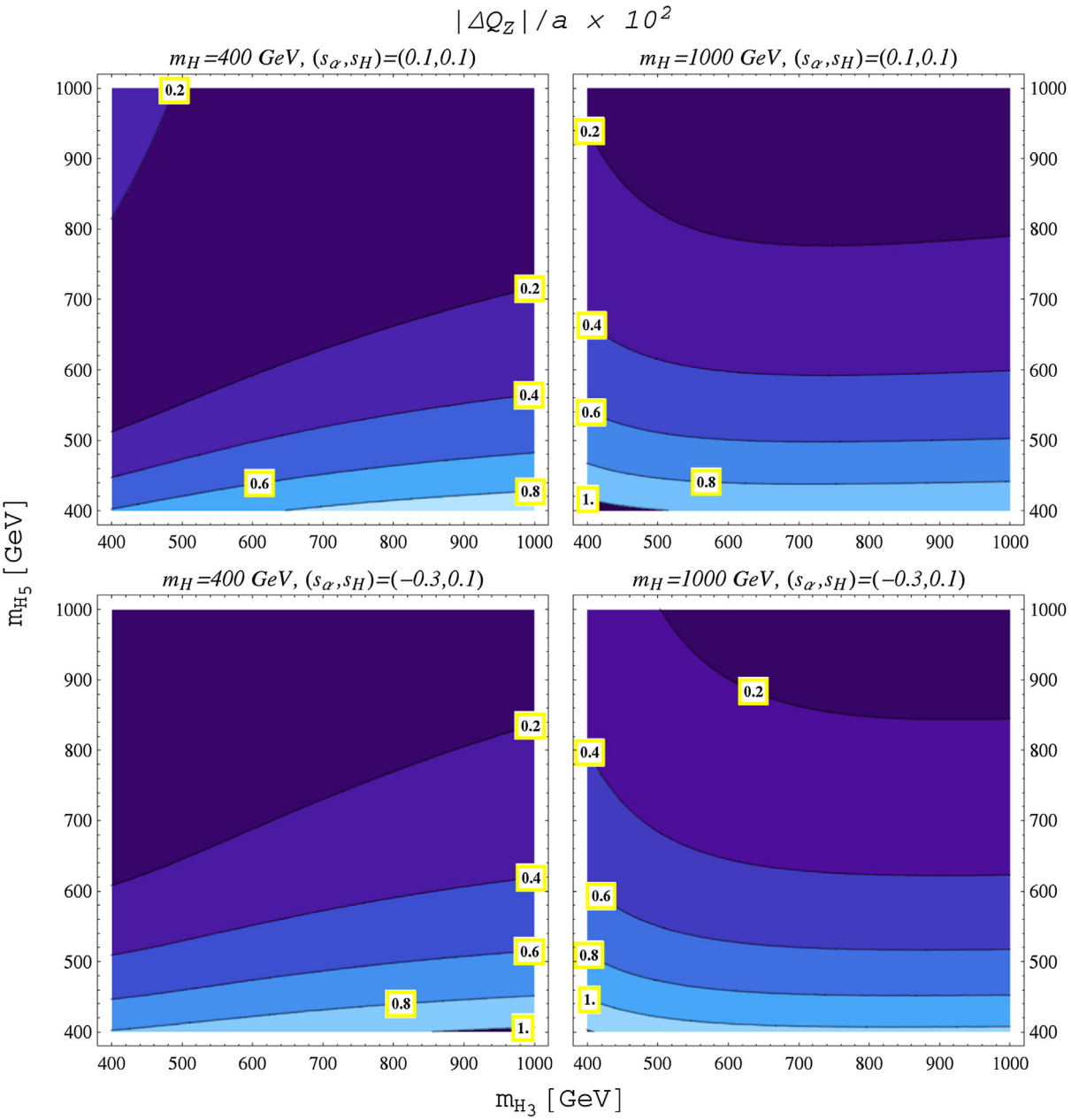

FIG. 10. The same as in Fig. 9, but for the ΔQ_Z form factor.

bosons are light, the type-(a) contributions numbers 2 and 3 are of a similar size as contributions 6, 8, and 10, whereas all other contributions are suppressed due to the small value of the corresponding coefficient C_Z^a. If m_H and m_{H_3} remain small while m_{H_5} increases, there is a cancellation between type-(a) contributions involving singlet and triplet scalar bosons, such that the total sum decreases considerably when m_{H_5} increases. In general the largest contributions are of the order of 1% of a in the region of the parameter space considered.

As in the case of the $WW\gamma$ form factors, we also note that the $\Delta\kappa_Z'$ form factor is about two orders of magnitude larger than ΔQ_Z. As it was pointed out above, this behavior can be explained in the context of the decoupling theorem.

V. CONCLUSIONS

The presence of new scalar particles is a consequence of well-motivated extensions of the SM. Even if such particles were not directly produced at particle colliders, their quantum effects could be at the reach of detection through precision measurement. In this work, we have obtained the one-loop corrections to the $\Delta\kappa_V'$ and ΔQ_V

($V = \gamma, Z$) form factors induced by new scalar particles. A model-independent calculation was done via both the Feynman parameter technique and the Passarino-Veltman reduction scheme. Our general results are expressed in terms of three (six) generic contributions to $\Delta\kappa'_\gamma$ and ΔQ_γ ($\Delta\kappa'_Z$ and ΔQ_Z) that can be used to calculate the corrections arising from models with an extended scalar sector predicting new neutral, singly, and doubly charged scalar bosons. For the numerical analysis we have focused on the GMM, which is a Higgs triplet model that has been the source of some interest recently. This model predicts 9 new scalar bosons accommodated in a singlet, a triplet, and a fiveplet, which yield 15 new contributions to $\Delta\kappa'_\gamma$ and ΔQ_γ, whereas $\Delta\kappa'_Z$ and ΔQ_Z receive 28 contributions. The general behavior of the $\Delta\kappa'_V$ and ΔQ_V form factors was analyzed for values of the parameters lying inside the region allowed by experimental and theoretical constraints. It was found that $\Delta\kappa'_V$ reaches values of the order of $a = g^2/(96\pi^2)$, with the largest values arising from the diagrams with two nondegenerate scalar bosons provided that there is a large splitting between their masses. On the other hand ΔQ_V reaches values of the order of 1% of a, with the largest contributions arising from diagrams with relatively light degenerate scalar bosons. Both form factors decrease rapidly when all the scalar boson masses are heavy. The values for $\Delta\kappa'_V$ and ΔQ_V predicted by the GMM are competitive with the ones predicted by other weakly coupled SM extensions, but a very high experimental precision still would be necessary to disentangle such effects.

ACKNOWLEDGMENTS

We acknowledge financial support from Sistema Nacional de Investigadores (Mexico), Consejo Nacional de Ciencia y Tecnología (Mexico) and Vicerrectoría de Investigación y Estudios de Posgrado (BUAP).

APPENDIX A: FEYNMAN RULES FOR THE GMM VERTICES

We now present the Feynman rules for the vertices of the type $X_A X_A V$, $\phi_A \phi_B X_C$, and $\phi_A X_B X_C$ arising in the GMM. Here X represents a neutral or charged gauge boson, $V = \gamma$, Z, and ϕ is a neutral, singly, or doubly charged scalar boson. The respective Lorentz structure for each vertex of this kind was shown in Fig. 2, so we only need to present the respective coupling constants. Since in the GMM there are no extra gauge bosons, the only vertices of the type $X_A X_A V$ are $W^\mp W^\pm \gamma$ and $W^\mp W^\pm Z$, whose coupling constants are $g_{WW\gamma} = g_\gamma = e$ and $g_{WWZ} = g_Z = g c_W$. As far as vertices of the class $\phi_A \phi_B X_C$ are concerned, the respective coupling constants are shown in Table I, whereas the coupling constants for vertices of the kind $\phi_A X_B X_C$ are presented in Table II.

TABLE I. Coupling constants for vertices of the class $\phi_A \phi_B X_C$ (two scalar bosons and one gauge boson) in the GMM. Here $s_H = \sin\theta_H$ and $c_H = \cos\theta_H$, $g_h = \frac{1}{6}(2\sqrt{6} c_H s_\alpha + 3 s_H c_\alpha)$, and $g_H = \frac{1}{6}(2\sqrt{6} c_H c_\alpha - 3 s_H s_\alpha)$. For the Lorentz structure see Fig. 2.

Vertex	Coupling constant
$H_3^\pm h W^\mp$	$g g_h$
$H_3^\pm H W^\mp$	$g g_H$
$H_3^\pm H_5^0 W^\mp$	$-\frac{\sqrt{3}}{6} g c_H$
$H_5^\pm H_5^0 W^\mp$	$\frac{\sqrt{3}}{2} g$
$H_5^\pm H_3^0 W^\mp$	$\pm \frac{i}{2} g c_H$
$H_3^\pm H_3^0 W^\mp$	$\pm \frac{i}{2} g$
$H_5^{\pm\pm} H_5^\mp W^\mp$	$-\frac{1}{\sqrt{2}} g$
$H_5^{\pm\pm} H_3^\mp W^\mp$	$-\frac{1}{\sqrt{2}} g c_H$
$H_3^0 h Z$	$i \frac{g}{c_W} g_h$
$H_3^0 H Z$	$-i \frac{g}{c_W} g_H$
$H_5^0 H_3^0 Z$	$-i \frac{g}{\sqrt{3} c_W} c_H$
$H_5^\pm H_3^\pm Z$	$\frac{g}{2 c_W} c_H$
$H_3^+ H_3^- Z$	$\frac{g}{2 c_W}(1 - 2 s_W^2)$
$H_5^+ H_5^- Z$	$\frac{g}{2 c_W}(1 - 2 s_W^2)$
$H_5^{++} H_5^{--} Z$	$\frac{g}{c_W}(1 - 2 s_W^2)$
$H_3^+ H_3^- \gamma$	e
$H_5^+ H_5^- \gamma$	e
$H_5^{++} H_5^{--} \gamma$	$2e$

TABLE II. Coupling constants for vertices of the class $\phi_A X_B X_C$ (one scalar boson and two gauge bosons) in the GMM. Here $f_h = \frac{1}{6}(3 c_H c_\alpha + 2\sqrt{6} s_H s_\alpha)$ and $f_H = \frac{1}{6}(3 c_H s_\alpha - 2\sqrt{6} s_H c_\alpha)$. For the Lorentz structure see Fig. 2.

Vertex	Coupling constant
$W^\pm W^\mp H_5^{\pm\pm}$	$\frac{g^2}{\sqrt{2}} v s_H$
$W^\pm Z H_5^\pm$	$\mp \frac{g^2}{2 c_W} v s_H$
$W^+ W^- H_5^0$	$\frac{g^2}{2\sqrt{3}} v s_H$
$ZZ H_5^0$	$-\frac{g^2}{\sqrt{3} c_W^2} v s_H$
$W^+ W^- h$	$-g^2 v f_h$
$W^+ W^- H$	$g^2 v f_H$
ZZh	$-\frac{g^2}{c_W^2} v f_h$
ZZH	$\frac{g^2}{c_W^2} v f_H$

APPENDIX B: ONE-LOOP FUNCTIONS

In this appendix we present the results for the loop integrals involved in the $\Delta\kappa'_V$ and ΔQ_V form factors in terms of parametric integrals and Passarino-Veltman scalar functions.

1. Parametric integrals

The loop functions arising from the Feynman diagrams of Fig. 3 can be written in terms of the following parametric integrals,

$$I^{V-i}_{\kappa,Q} = \int_0^1 F^{V-i}_{\kappa,Q}(x)dx, \tag{B1}$$

for $V = Z, \gamma$ and $i = a, b, c$. These loop functions depend on x_A, x_B, and x_V, but for the sake of shortness we will drop the explicit dependence from now on. It is worth reminding the reader that subscripts A, B correspond to the virtual particles circulating into each Feynman diagram of Fig. 3. We will first present the $F^{V-i}_{\kappa,Q}(x)$ functions for a massive neutral gauge boson V, which can be written as

$$F^{V-i}_{\kappa}(x) = f^i_0(x) + f^i_1(x)\tan^{-1}\left[\frac{(x-1)\sqrt{x_V}}{\zeta(x)}\right] + f^i_2(x)\log[\lambda(x)], \tag{B2}$$

and

$$F^{V-i}_{Q}(x) = h^i_0(x) + h^i_1(x)\tan^{-1}\left[\frac{(x-1)\sqrt{x_V}}{\zeta(x)}\right], \tag{B3}$$

where we introduced the auxiliary function

$$\zeta(x) = [4\lambda(x) - (x-1)^2 x_V]^{\frac{1}{2}}, \tag{B4}$$

with $\lambda(x) = x(x-\delta-1) + x_A$ and $\delta = x_A - x_B$. Also, $f^i_j(x)$ stand for polynomial functions given by

$$f^a_0(x) = 4(x^2-1), \tag{B5}$$

$$f^a_1(x) = -\frac{4}{\zeta(x)\sqrt{x_V}}((3x-1)(x-1)^2 x_V + 4\lambda(x)(x+1)), \tag{B6}$$

$$f^a_2(x) = 6x^2 - 8x + 2; \tag{B7}$$

$$f^b_0(x) = -\frac{1}{2x_A^2}(x-1)(x(x_V - 6x_A) + x_V), \tag{B8}$$

$$f^b_1(x) = \frac{1}{2\zeta(x)x_A^2\sqrt{x_V}}(4xx_V(x(x-\delta)+\delta_+) + 4x_A(x(x(7\delta - 8x + 9) - 11x_A + x_B - 1) + 4x_A) + (x-1)^2(3x-1)x_V^2), \tag{B9}$$

$$f^b_2(x) = \frac{1}{4x_A^2}((4-3x)x - 1)x_V; \tag{B10}$$

$$f^c_0(x) = \frac{1-x^2}{x_B}, \tag{B11}$$

$$f^c_1(x) = \frac{1}{\zeta(x)x_B\sqrt{x_V}}(4(x^2-1)(x-x_A) + 4x(x+3)x_B + (3x-1)(x-1)^2 x_V), \tag{B12}$$

$$f^c_2(x) = \frac{(4-3x)x - 1}{2x_B}, \tag{B13}$$

where we have defined $\delta_\pm = x_A \pm x_B - 1$.

As far as the polynomial functions h^j_i are concerned, we only need h^a_i,

$$h^a_0(x) = -\frac{8(x-1)x}{x_V}, \tag{B14}$$

$$h^a_1(x) = \frac{32\lambda x}{\zeta(x)x_V^{3/2}}, \tag{B15}$$

since the I^{V-b}_Q and I^{V-c}_Q loop functions obey

$$I^{V-b}_Q = \frac{2x_A - x_V}{8x_A^2} I^{V-a}_Q, \tag{B16}$$

$$I^{V-c}_Q = -\frac{1}{x_B} I^{V-a}_Q. \tag{B17}$$

As far as the coupling constants C^i_V are concerned, they are as follows:

$$C^a_V = \frac{g_{\phi_A\phi_B W} g_{\phi_B\phi_A W} g_{\phi_A\phi_A V}}{g_V}, \tag{B18}$$

$$C^b_V = \frac{g^2_{X_A\phi_B W} g_{X_A X_A V}}{m_W^2 g_V}, \tag{B19}$$

$$C^c_V = \frac{g^2_{\phi_A X_B W} g_{\phi_A\phi_A V}}{m_W^2 g_V}, \tag{B20}$$

where g_{ABC} stands for the coupling constants associated with the ABC vertex, which are presented in Appendix A. Notice that it is necessary to be careful when establishing the flow of the 4-momenta in the Feynman rule for each vertex to determine the correct sign of the respective coupling constant.

The contributions to $\Delta\kappa'^i_Z$ and ΔQ^i_Z from this set of diagrams follow easily after setting $x_V \to x_Z$ in the above parametric integrals and inserting the appropriate coupling constants in the coefficients C^i_V given in Eqs. (B18)–(18).

We can also obtain the electromagnetic form factors $\Delta\kappa_\gamma^{\prime i}$ and ΔQ_γ^i straightforwardly by considering the $x_V \to 0$ limit and the corresponding coupling constants. In this case, the parametric integrals simplify to

$$I_\kappa^{\gamma-a} = 2\int_0^1 (x-1)(3x-1)\log[\lambda(x)]dx, \tag{B21}$$

$$I_\kappa^{\gamma-b} = -\int_0^1 \frac{(x-1)^2(x^2+3x_A+\lambda(x))}{2x_A\lambda(x)}dx, \tag{B22}$$

$$I_\kappa^{\gamma-c} = \frac{1}{2}\int_0^1 (x-1)\left[\frac{(1-3x)\log[\lambda(x)]}{x_B}+\frac{4x}{\lambda(x)}\right]dx, \tag{B23}$$

and

$$I_Q^{\gamma-a} = \frac{4}{3}\int_0^1 \frac{(x-1)^3 x}{\lambda(x)}dx, \tag{B24}$$

with

$$I_Q^{\gamma-b} = \frac{1}{4x_A} I_Q^{\gamma-a}, \tag{B25}$$

$$I_Q^{\gamma-c} = -\frac{1}{4x_B} I_Q^{\gamma-a}. \tag{B26}$$

We now present the parametric integrals for the loop functions of the Feynman diagrams of Fig. 4, which only contribute to the $\Delta\kappa_Z^{\prime i}$ and ΔQ_Z^i form factors. This time the superscript i stands for the whole contribution of diagrams i_1 and i_2, with $i = d, e, f$. The parametric integrals $I_{\kappa,Q}^{Z-i}$ are given by a similar expression to that of Eq. (B1), but with the $F_{\kappa,Q}^{Z-i}$ functions now depending also on the variable x_C. They are given by

$$F_\kappa^{Z-i}(x) = f_0^{Z-i}(x) + f_1^{Z-i}(x)\eta_1(x) + f_2^{Z-i}(x)\eta_2(x), \tag{B27}$$

and

$$F_Q^{Z-i}(x) = h_0^{Z-i}(x) + h_1^{Z-i}(x)\eta_1(x) + h_2^{Z-i}(x)\eta_2(x), \tag{B28}$$

where we introduced the auxiliary functions

$$\eta_1(x) = \tan^{-1}\left[\frac{2(x-1)x_Z}{1+\delta'^2-(x-1)^2x_Z^2}\right], \tag{B29}$$

$$\eta_2(x) = \log\left[\frac{\lambda'(x)}{\lambda(x)}\right], \tag{B30}$$

with $\lambda'(x) = x(x-\delta'-1)+x_C$ and $\delta' = x_C - x_B$. The f_j^i and h_j^i functions are given by

$$f_0^d(x) = 4(x-1)(3x-1)\log[\lambda(x)] + 8(x^2-1), \tag{B31}$$

$$\begin{aligned} f_1^d(x) = \frac{4}{\theta(x)x_Z}(&-2(x+1)x_Z(-x(x_A-2x_B+x_C+2) \\ &+ x_A + x_C + 2x^2) + (5x+1)\delta'^2 \\ &- (x-1)^2(3x-1)x_Z^2), \end{aligned} \tag{B32}$$

$$f_2^d(x) = \frac{2}{x_Z}(-(5x+1)x_A + 5xx_C + x_C + x(3x-4)x_Z + x_Z); \tag{B33}$$

$$f_0^e(x) = -\frac{(x-1)}{x_C}((3x-1)\log[\lambda(x)] + 2(x+1)), \tag{B34}$$

$$\begin{aligned} f_1^e(x) = \frac{1}{\theta(x)x_Cx_Z}(&2x_Z(x(-x(x_A-2x_B+x_C)+2x_B+x_C \\ &+ 2x^2-2)+x_A) - \delta'(5xx_A+x_A-5xx_C+x_C) \\ &+ (x-1)^2(3x-1)x_Z^2) \end{aligned} \tag{B35}$$

$$\begin{aligned} f_2^e(x) = \frac{1}{2x_Cx_Z}(&5xx_A + x_A - 5xx_C + x_C \\ &+ ((4-3x)x-1)x_Z); \end{aligned} \tag{B36}$$

$$\begin{aligned} f_0^f(x) = \frac{(x-1)}{2x_Ax_Bx_Z}(&2x_Z(x(3x_A+9x_B-1)-3x_B-1) \\ &+ x_A\delta' - (3x-1)(3x_B+1)x_Z\log[\lambda(x)]), \end{aligned} \tag{B37}$$

$$\begin{aligned} f_1^f(x) = \frac{1}{2\theta(x)x_Ax_Bx_Z^2}(&x_Z^2(x^2(x_A(8x_B+5x_C+16)+9x_A^2+22x_B(x_C-2x_B)+76x_B-2x_C) - 4x(x_A(5x_B+x_C) \\ &+ 3x_A^2 + x_B(-3x_B+7x_C+2)+1) - 4x^3(4x_A+13x_B-1) - x_Ax_C + 3x_A^2 + 6x_Bx_C + 2x_C) \\ &+ x_Z\delta'(x_C(x(-4x_A-13x_B+5)-2x_A+3x_B+1)+x_A(x(10x_A+7x_B-8x+1)-4x_A+3x_B+1)) \\ &+ x_A\delta'^3 + (x-1)^2(3x-1)(3x_B+1)x_Z^3), \end{aligned} \tag{B38}$$

$$f_2^f(x) = -\frac{1}{4x_A x_B x_Z^2}(x_Z(-x_C(x(5x_A+13x_B-5)+x_A-3x_B)+3(3x+1)x_A x_B+(3x-1)x_A(3x_A-2x-1)+x_C) + x_A\delta'^2+(x-1)(3x-1)(3x_B+1)x_Z^2), \tag{B39}$$

with

$$\theta(x) = 2x_A(x_C-(x-1)x_Z)-x_A^2+4x(x_B+x-1)x_Z-(x_C+(x-1)x_Z)^2. \tag{B40}$$

Again we only need the h_i^d functions

$$h_0^d(x) = -\frac{16(x-1)x}{x_Z}, \tag{B41}$$

$$h_1^d(x) = -\frac{16x(\delta'^2-x_Z(x_A+x_C+2x^2-x(x_A-2x_B+x_C+2)))}{\theta(x)x_Z^2}, \tag{B42}$$

$$h_2^d(x) = \frac{8x\delta'}{x_Z^2}, \tag{B43}$$

whereas the loop functions for the type-(e) and type-(f) contributions are given by

$$I_Q^{Z-e} = -\frac{1}{4x_C} I_Q^{Z-d} \tag{B44}$$

$$I_Q^{Z-f} = \frac{\delta_+}{8x_A x_B} I_Q^{Z-d}. \tag{B45}$$

Finally, the C_Z^i coupling constants are

$$C_Z^d = \frac{g_{\phi_A\phi_B W} g_{\phi_B\phi_C W} g_{\phi_C\phi_A Z}}{g_Z}, \tag{B46}$$

$$C_Z^e = \frac{g_{\phi_A\phi_B W} g_{\phi_B X_C W} g_{X_C\phi_A Z}}{m_W^2 g_Z}, \tag{B47}$$

$$C_Z^f = \frac{g_{X_A X_B W} g_{X_B\phi_C W} g_{\phi_C X_A Z}}{m_W^2 g_Z}. \tag{B48}$$

2. Passarino-Veltman scalar integrals

The loop functions $I_{\kappa,Q}^{V-i}$ were also obtained via the Passarino-Veltman reduction scheme in terms of two- and three-point scalar functions with the help of the Feyncalc package [47]. We first define the following dimensionless ultraviolet finite functions:

$$\Delta_1 = B_0(0,m_A^2,m_A^2)-B_0(0,m_B^2,m_B^2), \tag{B49}$$

$$\Delta_2 = B_0(m_W^2,m_A^2,m_B^2)-B_0(0,m_B^2,m_B^2), \tag{B50}$$

$$\Delta_3 = B_0(m_V^2,m_A^2,m_A^2)-B_0(m_W^2,m_A^2,m_B^2), \tag{B51}$$

$$\Delta_4 = B_0(0,m_B^2,m_B^2)-B_0(0,m_C^2,m_C^2), \tag{B52}$$

$$\Delta_5 = B_0(m_W^2,m_B^2,m_C^2)-B_0(0,m_C^2,m_C^2), \tag{B53}$$

$$\Delta_6 = B_0(m_V^2,m_A^2,m_C^2)-B_0(m_W^2,m_B^2,m_C^2), \tag{B54}$$

$$\Delta_7 = m_W^2 C_0(0,m_W^2,m_W^2,m_A^2,m_A^2,m_B^2), \tag{B55}$$

$$\Delta_8 = m_W^2 C_0(m_V^2,m_W^2,m_W^2,m_A^2,m_C^2,m_B^2), \tag{B56}$$

where $B_0(m_i^2,m_j^2,m_k^2)$ and $C_0(p_1^2,p_2^2,p_{12}^2,m_i^2,m_j^2,m_k^2)$ are two- and three-point scalar functions.

The $I_{\kappa Q}^{V-i}$ loop functions can be cast in the following form:

$$I_\kappa^{V-i} = \frac{1}{D_\kappa^{V-i}}\sum_{j=0}^{8} p_j^{V-i}\Delta_j + 2x_V I_Q^{V-i}, \tag{B57}$$

$$I_Q^{V-i} = \frac{1}{D_Q^{V-i}}\sum_{j=1}^{8} q_j^{V-i}\Delta_j, \tag{B58}$$

with $\Delta_0 = 1$ and $i = a,\ldots,f$. For simplicity we have omitted the dependence of the polynomial functions $D_{\kappa',Q}^{V-i}$, p_j^{V-i}, and q_j^{V-i} on x_A, x_B, and x_C.

For the Feynman diagrams of Fig. 3 we obtain the following nonvanishing polynomial functions for a massive neutral gauge boson V:

$$D_{\kappa'}^{V-a} = 3y_V^2 \tag{B59}$$

$$p_0^{V-a} = -2y_V(3\delta^2-x_V+1), \tag{B60}$$

$$p_1^{V-a} = -6x_A y_V \delta_-, \tag{B61}$$

$$p_2^{V-a} = 6\delta y_V \delta_-, \tag{B62}$$

$$p_3^{V-a} = 6(6\delta^2-x_A(x_V+8)+x_B(5x_V-8)+x_V+2), \tag{B63}$$

$$p_7^{V-a} = -12(\rho + x_B x_V)(3\delta - x_V + 1), \tag{B64}$$

$$D_{\kappa'}^{V-b} = 2x_A^2 y_V^2 \tag{B65}$$

$$p_0^{V-b} = -\frac{1}{6} y_V (2x_A - x_V)(3\delta^2 - x_V + 1), \tag{B66}$$

$$p_1^{V-b} = -\frac{1}{2} x_A y_V \delta_-(2x_A - x_V), \tag{B67}$$

$$p_2^{V-b} = \frac{1}{2} \delta y_V \delta_-(2x_A - x_V), \tag{B68}$$

$$\begin{aligned} p_3^{V-b} = \frac{1}{2}(&24x_A^2(2 - x_B - x_V) + x_A(22x_B x_V + 4x_B(3x_B - 4) + 5x_V^2 - 6x_V + 4) \\ &+ 12x_A^3 - x_V(x_B(6x_B + 5x_V - 8) + x_V + 2)), \end{aligned} \tag{B69}$$

$$\begin{aligned} p_7^{V-b} = &x_A^3(18x_B + 13x_V - 22) - 3x_A^2(9x_B x_V + 6(x_B - 2)x_B + x_V^2 + 3x_V - 10) \\ &+ x_A((9x_B + 4)x_V^2 + (x_B(17x_B - 16) - 5)x_V + 2(3x_B - 1)(x_B - 1)^2) \\ &- 6x_A^4 - x_V(3x_B + x_V - 1)(x_B(x_B + x_V - 2) + 1), \end{aligned} \tag{B70}$$

$$D_{\kappa'}^{V-c} = x_B y_V^2 \tag{B71}$$

$$p_0^{V-c} = \frac{1}{6} y_V (3\delta^2 - x_V + 1), \tag{B72}$$

$$p_1^{V-c} = \frac{1}{2} x_A y_V \delta_-, \tag{B73}$$

$$p_2^{V-c} = -\frac{1}{2} y_V \delta \delta_-, \tag{B74}$$

$$\begin{aligned} p_3^{V-c} = \frac{1}{2}(&x_A(12x_B + x_V + 8) - 6x_A^2 \\ &+ 3x_B(-2x_B + x_V - 8) - x_V - 2), \end{aligned} \tag{B75}$$

$$\begin{aligned} p_7^{V-c} = &-x_A^2(9x_B + x_V + 5) + x_A(x_B(9x_B + x_V + 14) \\ &+ 2x_V + 1) + 3x_A^3 + x_B(-3x_B(x_B + 3) \\ &+ (x_V - 9)x_V + 11) - x_V + 1, \end{aligned} \tag{B76}$$

$$D_Q^{V-a} = \frac{3}{4} x_V y_V^3 \tag{B77}$$

$$q_0^{V-a} = y_V(12 - 2\delta^2(x_V + 6) + (x_V - 2)x_V), \tag{B78}$$

$$q_1^{V-a} = -2x_A y_V(\delta(x_V + 6) - 2(x_V + 1)), \tag{B79}$$

$$q_2^{V-a} = 2y_V(\delta^2(x_V + 6) - 2x_A(x_V + 1) + 2x_B(2x_V - 3)), \tag{B80}$$

$$\begin{aligned} q_3^{V-a} = &2(x_A(8 - x_V(3x_V + 20)) + 6\delta^2(3x_V - 2) \\ &+ 3x_B(x_V(3x_V - 4) + 8) \\ &+ 2(x_V - 1)(x_V + 6)), \end{aligned} \tag{B81}$$

$$\begin{aligned} q_7^{V-a} = &-6(-2x_A x_B \delta(9x_V - 6) - 2x_A^2(x_V(x_V + 4) - 2) \\ &+ 2x_A(2x_B(x_V(2x_V - 1) + 2) + x_V(2x_V - 1) + 2) \\ &+ x_A^3(6x_V - 4) - x_B x_V^3 + 2(-3x_B^2 + x_B - 1)x_V^2 \\ &+ 2(x_B(-3(x_B - 2)x_B - 5) + 2)x_V + 4(x_B - 1)^3), \end{aligned} \tag{B82}$$

with $y_V = 1 - 4x_V$, and $\rho = 1 - 2(x_A + x_B) + \delta^2$. Also, the I_Q^{V-b} and I_Q^{V-c} loop functions obey Eqs. (B16) and (15).

For $V = \gamma$, we need to be careful when taking the limit $x_V \to 0$ as one obtains an indeterminate result of the form $0/0$ since the Gram determinant vanishes. Therefore one must apply the l'Hôpital rule, as is described in detail in Ref. [44]. We obtain the following results after applying this method:

$$D_{\kappa'}^{\gamma-a} = 3 \tag{B83}$$

$$p_0^{\gamma-a} = 6\delta^2 - 3\delta - 1, \tag{B84}$$

$$p_1^{\gamma-a} = 6x_A \delta_-, \tag{B85}$$

$$p_2^{\gamma-a} = 6(x_A - \delta^2), \tag{B86}$$

$$D_{\kappa'}^{\gamma-b} = 2\rho^2 x_A \tag{B87}$$

$$p_0^{\gamma-b} = \frac{1}{6}(\rho(3\rho(2\delta^2 + 7x_A + x_B) + 96x_A x_B - \rho)), \tag{B88}$$

$$\begin{aligned} p_1^{\gamma-b} = \rho x_A(&x_A(-4x_B + \rho - 8) + 4x_A^2 \\ &- (\rho + 4)x_B - \rho + 4), \end{aligned} \tag{B89}$$

$$p_2^{\gamma-b} = -\rho(\rho(\delta^2+3x_A)+8x_Ax_B), \tag{B90}$$

$$D_{\kappa'}^{\gamma-c} = 2\rho^2 x_B \tag{B91}$$

$$p_0^{\gamma-c} = \frac{1}{6}(-\rho(\rho(-3x_A(4x_B+1)+6x_A^2+3x_B(2x_B+9)-1)+48x_B\delta_+)), \tag{B92}$$

$$p_1^{\gamma-c} = \rho x_A(1-\delta)(4x_B+\rho), \tag{B93}$$

$$p_2^{\gamma-c} = \rho(\rho(\delta^2-x_A+4x_B)+4x_B\delta_+), \tag{B94}$$

$$D_Q^{\gamma-a} = 3\rho \tag{B95}$$

$$q_0^{\gamma-a} = -\frac{2}{3}(-3x_A^3(8x_B+5)+x_A^2(9x_B(4x_B+3)+10) - x_A(x_B(3x_B(8x_B+3)+8)-1)+6x_A^4 + (x_B-1)(6x_B^3+3x_B^2+x_B+2)), \tag{B96}$$

$$q_1^{\gamma-a} = -4x_A(\delta-1)((\delta-1)^2-3x_B), \tag{B97}$$

$$q_2^{\gamma-a} = 4(-(4x_A+1)x_B^3+x_A(6x_A-1)x_B^2 + x_A((5-4x_A)x_A-1)x_B+(x_A-1)^3x_A+x_B^4), \tag{B98}$$

with the $I_Q^{\gamma-b}$ and $I_Q^{\gamma-c}$ obeying (B25) and (B26).

Finally we present the polynomial functions for the contributions to the WWZ form factors obtained from the diagrams of Fig. 4:

$$D_{\kappa'}^{Z-d} = x_Z y_Z^2 \tag{B99}$$

$$p_0^{Z-d} = \frac{1}{3}(-2y_Z(x_Z(3(-2x_Ax_B+x_A^2-2x_Bx_C+2x_B^2+x_C^2)+2)-6(x_A-x_C)^2-2x_Z^2)), \tag{B100}$$

$$p_1^{Z-d} = 2x_Ay_Z(-x_A(x_Z-2)+x_Bx_Z-2x_C+x_Z), \tag{B101}$$

$$p_2^{Z-d} = 2x_Z(x_A(17x_B-3x_C+5)-7x_A^2+x_B(-10x_B+3x_C+4)+7x_C-2) + 4(x_A-x_C)(3x_A-6x_B+3x_C+2)+2x_Z^2(\delta^2-4x_B-1), \tag{B102}$$

$$p_4^{Z-d} = -2(-x_A(3x_B(3x_Z-4)-5x_Cx_Z+8x_C+x_Z^2+x_Z+4)+x_A^2(x_Z+2) + x_C(x_B(-x_Z^2+x_Z-12)-7x_Z+4)+x_Z((x_B+6)x_Bx_Z+2(x_B-6)x_B+x_Z+2)+6x_C^2), \tag{B103}$$

$$p_5^{Z-d} = 2x_Z^2(-x_A-2x_B(x_C-3)+x_B^2+(x_C-1)x_C+1) + 2x_Z(x_A(-9x_B+7x_C-1)+x_A^2+5x_Bx_C+2(x_B-6)x_B-6x_C^2-3x_C+2) + 4(x_A-x_C)(x_A+6x_B-7x_C-2), \tag{B104}$$

$$p_6^{Z-d} = 2(x_A(2x_C(5x_Z-8)-x_Z(12x_B+x_Z+8))+x_A^2(x_Z+8)-x_Cx_Z(12x_B+x_Z+8) + 2x_Z(x_B(6x_B+5x_Z-8)+x_Z+2)+x_C^2(x_Z+8)), \tag{B105}$$

$$p_8^{Z-d} = -4(3x_A-6x_B+3x_C-2x_Z+2)(-x_Z(x_A(x_B-x_C+1)+x_B(-x_B+x_C+2)+x_C) + (x_A-x_C)^2+x_Bx_Z^2+x_Z); \tag{B106}$$

$$D_{\kappa'}^{Z-e} = x_Cx_Z^2y_Z^3 \tag{B107}$$

$$p_0^{Z-e} = \frac{1}{6}(-x_Zy_Z^2(-x_Z(3(-2x_Ax_B+x_A^2-2x_Bx_C+2x_B^2+x_C^2)+2)+6(x_A-x_C)^2+2x_Z^2)), \tag{B108}$$

$$p_1^{Z-e} = \frac{1}{2}(x_Ax_Zy_Z^2(x_A(x_Z-2)-(x_B+1)x_Z+2x_C)), \tag{B109}$$

$$p_2^{Z-e} = -\frac{1}{2}x_Z y_Z (x_A (x_B ((17-2x_Z)x_Z - 12) - 3x_C x_Z + 5x_Z + 4) + x_A^2 (x_Z - 6)(x_Z - 1) + 3x_C ((x_B + 5)x_Z + 4(x_B - 3)) + x_Z (x_B (x_B (x_Z - 10) - 4x_Z + 4) - x_Z - 2) - 6x_C^2), \tag{B110}$$

$$p_4^{Z-e} = -\frac{1}{2}x_Z y_Z (x_A (3x_B (3x_Z - 4) - 5x_C x_Z + 8x_C + x_Z^2 + x_Z + 4) + x_A^2 (-(x_Z + 2)) + x_C (x_B ((x_Z - 1)x_Z + 12) + 15x_Z - 36) - x_Z ((x_B + 6)x_B x_Z + 2(x_B - 6)x_B + x_Z + 2) - 6x_C^2), \tag{B111}$$

$$p_5^{Z-e} = \frac{1}{2}x_Z y_Z (x_A (3x_B (3x_Z - 4) - 7x_C x_Z + 16x_C + x_Z^2 + x_Z + 4) + x_A^2 (-(x_Z + 2)) + x_C (x_B (x_Z (2x_Z - 5) + 12) + x_Z (x_Z + 11) - 36) - x_Z ((x_B + 6)x_B x_Z + 2(x_B - 6)x_B + x_Z + 2) - x_C^2 ((x_Z - 6)x_Z + 14)), \tag{B112}$$

$$p_6^{Z-e} = \frac{1}{2}x_Z y_Z (x_A (x_Z (12x_B + x_Z + 8) + 2x_C (8 - 5x_Z)) + x_A^2 (-(x_Z + 8)) + x_C x_Z (12x_B + 5x_Z - 8) - 2x_Z (x_B (6x_B + 5x_Z - 8) + x_Z + 2) - x_C^2 (x_Z + 8)), \tag{B113}$$

$$p_8^{Z-e} = -x_Z y_Z (x_A^2 (3x_B (x_Z + 2) - 3x_C x_Z + 3x_C + 5x_Z - 2) + x_A (4x_C (3x_B (x_Z - 1) + (x_Z - 3)x_Z + 5) - x_Z (x_B (9x_B + 5x_Z - 2) + 2x_Z + 1) - 3x_C^2 (x_Z - 1)) - 3x_A^3 + x_C x_Z (x_B (-9x_B - 7x_Z + 10) - 4x_Z + 7) + 3x_C^2 (x_B x_Z + 2x_B + 3x_Z - 6) + 2x_Z (3x_B + x_Z - 1)(x_B (x_B + x_Z - 2) + 1) - 3x_C^3); \tag{B114}$$

$$D_{\kappa'}^{Z-f} = 4x_A x_B x_Z y_Z^2 \tag{B115}$$

$$p_0^{Z-f} = -\frac{1}{3}y_Z \delta_+ (x_Z (3(-2x_A x_B + x_A^2 - 2x_B x_C + 2x_B^2 + x_C^2) + 2) - 6(x_A - x_C)^2 - 2x_Z^2), \tag{B116}$$

$$p_1^{Z-f} = -x_A y_Z \delta_+ (x_A (x_Z - 2) - (x_B + 1)x_Z + 2x_C), \tag{B117}$$

$$p_2^{Z-f} = x_A^3 (x_Z - 6)(x_Z - 1) - x_A^2 (x_B ((x_Z - 10)x_Z + 6) + 3x_Z (x_C - x_Z + 4) - 30) + x_A (x_Z (x_B (7x_B + 64) + 10x_C + 17) - 2(x_B (40 - 6x_C) + 6x_B^2 + x_C (3x_C + 2) + 18) - (x_B (x_B + 14) + 5)x_Z^2) + (x_B - 1)(x_C (3x_B (x_Z + 4) + 7x_Z - 4) - x_Z (x_B (x_B (x_Z - 10) + 4(x_Z - 7)) - x_Z - 2) - 6x_C^2), \tag{B118}$$

$$p_4^{Z-f} = x_A^3 (-(x_Z + 2)) - x_A^2 (2x_B (4x_Z - 7) + 5x_Z (x_Z - x_C) + 8x_C - 22x_Z + 38) + x_A (x_B (x_C ((x_Z - 6)x_Z + 20) + (76 - 17x_Z)x_Z - 80) + x_B^2 (-(x_Z - 4))(x_Z - 3) - 6(x_C - x_Z)^2 - 12(x_C + 3) + 21x_Z) + (x_B - 1)(x_C (x_B (-x_Z^2 + x_Z - 12) - 7x_Z + 4) + x_Z (x_B (x_B (x_Z + 2) - 2x_Z + 20) + x_Z + 2) + 6x_C^2), \tag{B119}$$

$$p_5^{Z-f} = x_A^3 (x_Z + 2) + x_A^2 (x_B (14 - 8x_Z) + x_C (7x_Z - 16) + (22 - 5x_Z)x_Z - 38) + x_A (x_B (-2x_C ((x_Z - 6)x_Z + 14) + x_Z (17x_Z - 76) + 80) + x_B^2 (x_Z - 4)(x_Z - 3) + x_C^2 ((x_Z - 6)x_Z + 14) - x_C (x_Z (x_Z + 10) - 20) + 3x_Z (2x_Z - 7) + 36) + (x_B - 1)(-x_C (x_B (x_Z (2x_Z - 5) + 12) + (x_Z - 1)(x_Z + 4)) + x_Z (x_B (x_B (x_Z + 2) - 2x_Z + 20) + x_Z + 2) + x_C^2 ((x_Z - 6)x_Z + 14)), \tag{B120}$$

$$p_6^{Z-f} = x_Z^2 (x_A (21x_B - x_C + 7) - 5x_A^2 - (x_B - 1)(6x_B + x_C - 2)) + x_Z (x_C^2 \delta_+ + 2x_C (5x_A - 6x_B - 4)\delta_+ - 11x_A^2 x_B - 60x_A x_B + x_A^3 + 7x_A^2 - 4x_A + 12x_B^3 + 36x_B^2 - 44x_B) + 8\delta_+ (x_A - x_C)^2 - 4x_Z, \tag{B121}$$

$$
\begin{aligned}
p_8^{Z-f} = &-2(x_A(x_C(-3x_B^2y_Z + x_B(x_Z(9x_Z-26)+32) + x_Z(6x_Z-11)+20) \\
&+ x_C^2(-9x_B-8x_Z+5) + x_Z(x_B(x_B(43-13x_Z)+3x_B^2 - x_Z(2x_Z+1)+9) - 6x_Z+9) + 3x_C^3) \\
&- 3x_A^3(x_Z(x_B-x_C+3)+x_B+x_C-5) + x_A^2(x_B(-9x_Cx_Z+9x_C+7x_Z^2-40)+6x_B^2(x_Z-1) \\
&- 4(x_C-1)x_Z^2 + 3x_C(x_C+3)x_Z - x_C(3x_C+17)+2(x_Z-9)) + 3x_A^4 \\
&+ (x_B-1)(-x_C^2(3x_B(x_Z+2)+5x_Z-2) + x_Cx_Z(x_B(9x_B+x_Z+14)+2x_Z+1) \\
&- 2x_Z(x_B(3x_B(x_B+3)-(x_Z-9)x_Z-11)+x_Z-1)+3x_C^3)); \qquad \text{(B122)}
\end{aligned}
$$

$$
D_Q^{Z-d} = \frac{3}{8}x_Z^2y_Z^3 \qquad \text{(B123)}
$$

$$
\begin{aligned}
q_0^{Z-d} = &\, y_Z(2x_A(x_Bx_Z(x_Z+6)+x_C(16-9x_Z)) + x_A^2(-((x_Z-3)x_Z+16)) \\
&+ 2x_Bx_Cx_Z(x_Z+6) + x_Z(-2x_B^2(x_Z+6)+(x_Z-2)x_Z+12) - x_C^2((x_Z-3)x_Z+16)), \qquad \text{(B124)}
\end{aligned}
$$

$$
q_1^{Z-d} = -x_Ay_Z(x_A((x_Z-3)x_Z+16) - x_Z(x_Bx_Z+6x_B+2x_Z+2) + x_C(9x_Z-16)), \qquad \text{(B125)}
$$

$$
\begin{aligned}
q_2^{Z-d} = &-2x_Z^2(x_A(-13x_B+3x_C-1)+5x_A^2-3(x_B+4)x_C+8x_B^2+5x_B+5) \\
&- 6x_Z(x_A(5x_B+x_C-9)-3x_A^2-9x_Bx_C+2x_B^2+x_C(4x_C+9)-2) \\
&+ 36(x_C-x_A)(x_A-2x_B+x_C+2) + x_Z^3(-2x_Ax_B+x_A^2+x_A+(x_B-5)x_B-2), \qquad \text{(B126)}
\end{aligned}
$$

$$
\begin{aligned}
q_4^{Z-d} = &\, x_Z^3(3x_A+x_B(-x_B+x_C-13)-2) \\
&+ x_Z^2(x_A(30x_B-15x_C-4)-3x_A^2+2x_B(-10x_B+4x_C+17)+24x_C-10) \\
&+ 2x_Z(x_A(23(x_C+1)-39x_B)-5x_A^2+3(x_B(5x_C-8)+6x_B^2-x_C(4x_C+9)+2)) \\
&+ 4(x_A-x_C)(7x_A+18x_B-9x_C-18), \qquad \text{(B127)}
\end{aligned}
$$

$$
\begin{aligned}
q_5^{Z-d} = &\, x_Z^3(-3x_A-2(x_B+1)x_C+x_B^2+13x_B+x_C^2+2) \\
&+ x_Z^2(x_A(-30x_B+24x_C+4)+3x_A^2-2x_B(5x_C+17)+20x_B^2-x_C(7x_C+18)+10) \\
&+ 2x_Z(x_A(39x_B-49x_C-23)+5x_A^2-3x_B(x_C-8)-18x_B^2+x_C(26x_C+31)-6) \\
&- 4(x_A-x_C)(7x_A+18x_B-25x_C-18), \qquad \text{(B128)}
\end{aligned}
$$

$$
\begin{aligned}
q_6^{Z-d} = &\, x_Z^2(x_A(-36x_B+30x_C-20)+3x_A^2-12x_B(3x_C+2)+36x_B^2+x_C(3x_C-20)+20) \\
&+ 2x_Z(2x_A(6x_B-23x_C+2)+17x_A^2+4(3x_B+1)x_C-12(x_B-1)^2+17x_C^2) \\
&- 64(x_A-x_C)^2 + x_Z^3(-3x_A+18x_B-3x_C+4), \qquad \text{(B129)}
\end{aligned}
$$

$$
\begin{aligned}
q_8^{Z-d} = &-6(2x_Z^3(2x_Ax_B-x_Ax_C+x_A+2x_Bx_C-3x_B^2+x_B+x_C-1) \\
&- x_Z^2(3x_A^2(x_B-x_C+2)+x_A(2x_B(6x_C+1)-9x_B^2-x_C(3x_C+4)+1) \\
&+ 3(x_B+2)x_C^2+(2-9x_B)x_Bx_C+2x_B(3(x_B-2)x_B+5)+x_C-4) \\
&+ 2x_Z(-3x_A^2(x_B+x_C-2)+x_A(2x_B(6x_C+1)-3x_B^2-x_C(3x_C+10)+1) \\
&+ 2x_A^3-3x_B^2(x_C+2)+x_B((2-3x_C)x_C+6)+2x_B^3+x_C+2x_C^2(x_C+3)) \\
&- 6(x_A-x_C)^2(x_A-2x_B+x_C+2) - x_Bx_Z^4-4x_Z), \qquad \text{(B130)}
\end{aligned}
$$

with the I_Q^{Z-e} and I_Q^{Z-f} functions given by (B44) and (B45).

TABLE III. C_V^a coefficients for all the type-(a) contributions to the $\Delta\kappa_V'$ and ΔQ_V form factors in the GMM. The second column shows the particles circulating into the loop and the last two columns show the corresponding C_V^a factors.

Number	AB	C_Z^a	C_γ^a
1	$H_3^- h$	$\frac{g^2}{2c_W^2} g_h^2 (1-2s_W^2)$	$g^2 g_h^2$
2	$H_3^- H$	$\frac{g^2}{2c_W^2} g_H^2 (1-2s_W^2)$	$g^2 g_H^2$
3	$H_3^- H_3^0$	$\frac{g^2}{8c_W^2}(1-2s_W^2)$	$\frac{g^2}{4}$
4	$H_3^- H_5^0$	$\frac{g^2 c_H^2}{24c_W^2}(1-2s_W^2)$	$\frac{1}{12} g^2 c_H^2$
5	$H_5^- H_3^0$	$\frac{g^2 c_H^2}{8c_W^2}(1-2s_W^2)$	$\frac{1}{4} g^2 c_H^2$
6	$H_5^- H_5^0$	$\frac{3g^2}{8c_W^2}(1-2s_W^2)$	$\frac{3}{4} g^2$
7	$H_3^+ H_5^{++}$	$-\frac{g^2 c_H^2}{4c_W^2}(1-2s_W^2)$	$-\frac{1}{2} g^2 c_H^2$
8	$H_5^+ H_5^{++}$	$-\frac{g^2}{4c_W^2}(1-2s_W^2)$	$-\frac{1}{2} g^2$
9	$H_5^{--} H_3^-$	$\frac{g^2 c_H^2}{2c_W^2}(1-2s_W^2)$	$g^2 c_H^2$
10	$H_5^{--} H_5^-$	$\frac{g^2}{2c_W^2}(1-2s_W^2)$	g^2

TABLE IV. The same as in Table III, but for the type-(b) contributions.

Number	AB	C_Z^b	C_γ^b
1	$W^- H$	$-g^4 \frac{f_H^2 v^2}{m_W^2}$	$g^4 \frac{f_H^2 v^2}{m_W^2}$
2	$W^- H_5^0$	$-\frac{g^4 s_H^2 v^2}{12 m_W^2}$	$\frac{g^4 s_H^2 v^2}{12 m_W^2}$
3	$W^+ H_5^{++}$	$\frac{g^4 s_H^2 v^2}{2 m_W^2}$	$-\frac{g^4 s_H^2 v^2}{2 m_W^2}$

TABLE V. The same as in Table III, but for the type-(c) contributions.

Number	AB	C_Z^c	C_γ^c
1	$H_5^- Z$	$\frac{g^4 s_H^2 v^2}{8 c_W^4 m_W^2}(1-2s_W^2)$	$\frac{g^4 s_H^2 v^2}{4 c_W^2 m_W^2}$
2	$H_5^{--} W^-$	$-\frac{g^4 s_H^2 v^2}{2 c_W^2 m_W^2}(1-2s_W^2)$	$-\frac{g^4 s_H^2 v^2}{m_W^2}$

TABLE VI. C_Z^d coefficients for the type-(d) contributions in the GMM. The second column shows the particles circulating into the loop and the last column shows the corresponding C_Z^d factor.

Number	ABC	C_Z^d
1	$H_3^- H_3^0 H_5^-$	$\frac{g^2 c_H^2}{8 c_W^2}$
2	$H_3^- H_5^0 H_5^-$	$\frac{g^2 c_H^2}{8 c_W^2}$
3	$H_3^+ H_5^{++} H_5^+$	$-\frac{g^2 c_H^2}{4 c_W^2}$
4	$H_3^0 H_3^+ h$	$\frac{g^2}{2 c_W^2} g_h^2$
5	$H_3^0 H_3^+ H$	$-\frac{g^2}{2 c_W^2} g_H^2$
6	$H_3^0 H_3^+ H_5^0$	$\frac{g^2 c_H^2}{12 c_W^2}$
7	$H_3^0 H_5^+ H_5^0$	$-\frac{g^2 c_H^2}{4 c_W^2}$

TABLE VII. The same as in Table VI, but for the type-(e) contributions.

Number	ABC	C_Z^e
1	$H_5^- H_5^0 W^-$	$-\frac{g^4 s_H^2 v^2}{8 c_W^2 m_W^2}$
2	$H_5^+ H_5^{++} W^+$	$\frac{g^4 s_H^2 v^2}{\sqrt{24} c_W^2 m_W^2}$
3	$H_5^0 H_5^+ Z$	$\frac{g^4 s_H^2 v^2}{4 c_W^4 m_W^2}$

TABLE VIII. The same as in Table VI, but for the type-(f) contributions.

Number	ABC	C_Z^f
1	$W^- Z H_5^-$	$-\frac{g^4 s_H^2 v^2}{4 c_W^2 m_W^2}$
2	$Z W^+ H$	$-\frac{g^4 v^2}{c_W^2 m_W^2} f_H^2$
3	$Z W^+ H_5^0$	$-\frac{g^4 s_H^2 v^2}{6 c_W^2 m_W^2}$

APPENDIX C: C_V^i COEFFICIENTS FOR ALL THE NEW CONTRIBUTIONS OF THE GMM TO THE $\Delta\kappa_\gamma'$ AND ΔQ_γ FORM FACTORS

After taking into account all the vertices allowed in the GMM (Appendix A) we can determine the new contributions to the $\Delta\kappa_V'$ and ΔQ_V form factors arising from the Feynman diagrams of Figs. 3 and 4. In Tables III–VIII we show the explicit form of the C_V^i coefficients of Eqs. (B18)–(18) and (B46)–(B48) for each such contribution.

[1] S. Chatrchyan *et al.* (CMS Collaboration), Phys. Lett. B **716**, 30 (2012).
[2] G. Aad *et al.* (ATLAS Collaboration), Phys. Lett. B **716**, 1 (2012).
[3] H. Georgi and M. Machacek, Nucl. Phys. **B262**, 463 (1985).
[4] J. Gunion, R. Vega, and J. Wudka, Phys. Rev. D **42**, 1673 (1990).
[5] A. Delgado, M. Garcia-Pepin, M. Quiros, J. Santiago, and R. Vega-Morales, J. High Energy Phys. 06 (2016) 042.
[6] S. I. Godunov, M. I. Vysotsky, and E. V. Zhemchugov, Phys. Lett. B **751**, 505 (2015).
[7] C.-W. Chiang and K. Tsumura, J. High Energy Phys. 04 (2015) 113.
[8] K. Hartling, K. Kumar, and H. E. Logan, arXiv:1412.7387.
[9] S. I. Godunov, M. I. Vysotsky, and E. V. Zhemchugov, J. Exp. Theor. Phys. **120**, 369 (2015).
[10] C.-W. Chiang and T. Yamada, Phys. Lett. B **735**, 295 (2014).
[11] C. Englert, E. Re, and M. Spannowsky, Phys. Rev. D **87**, 095014 (2013).
[12] S. Godfrey and K. Moats, Phys. Rev. D **81**, 075026 (2010).
[13] H. E. Logan and V. Rentala, Phys. Rev. D **92**, 075011 (2015).
[14] K. Hartling, K. Kumar, and H. E. Logan, Phys. Rev. D **90**, 015007 (2014).
[15] C.-W. Chiang and K. Yagyu, J. High Energy Phys. 01 (2013) 026.
[16] C. Degrande, K. Hartling, H. E. Logan, A. D. Peterson, and M. Zaro, Phys. Rev. D **93**, 035004 (2016).
[17] C.-W. Chiang, A.-L. Kuo, and T. Yamada, J. High Energy Phys. 01 (2016) 120.
[18] C.-W. Chiang, S. Kanemura, and K. Yagyu, Phys. Rev. D **93**, 055002 (2016).
[19] W. A. Bardeen, R. Gastmans, and B. E. Lautrup, Nucl. Phys. **B46**, 319 (1972).
[20] G. Couture, J. N. Ng, J. L. Hewett, and T. G. Rizzo, Phys. Rev. D **36**, 859 (1987).
[21] A. B. Lahanas and V. C. Spanos, Phys. Lett. B **334**, 378 (1994).
[22] F. Larios, J. A. Leyva, and R. Martinez, Phys. Rev. D **53**, 6686 (1996).
[23] A. Flores-Tlalpa, J. Montano, H. Novales-Sanchez, F. Ramirez-Zavaleta, and J. J. Toscano, Phys. Rev. D **83**, 016011 (2011).
[24] A. Moyotl and G. Tavares-Velasco, J. Phys. G **37**, 105012 (2010).
[25] J. Montano, G. Tavares-Velasco, J. J. Toscano, and F. Ramirez-Zavaleta, Phys. Rev. D **72**, 055023 (2005).
[26] J. L. Garcia-Luna, G. Tavares-Velasco, and J. J. Toscano, Phys. Rev. D **69**, 093005 (2004).
[27] J. Hernandez-Sanchez, F. Procopio, G. Tavares-Velasco, and J. J. Toscano, Phys. Rev. D **75**, 073017 (2007).
[28] G. Tavares-Velasco and J. J. Toscano, J. Phys. G **30**, 1299 (2004).
[29] G. Tavares-Velasco and J. J. Toscano, Phys. Rev. D **69**, 017701 (2004).
[30] E. N. Argyres, A. B. Lahanas, C. G. Papadopoulos, and V. C. Spanos, Phys. Lett. B **383**, 63 (1996).
[31] F. Ramirez-Zavaleta, G. Tavares-Velasco, and J. J. Toscano, Phys. Rev. D **75**, 075008 (2007).
[32] K. Hagiwara, R. D. Peccei, D. Zeppenfeld, and K. Hikasa, Nucl. Phys. **B282**, 253 (1987).
[33] A. Arbey *et al.*, Eur. Phys. J. C **75**, 371 (2015).
[34] L. Bian, J. Shu, and Y. Zhang, J. High Energy Phys. 09 (2015) 206.
[35] G. Passarino and M. J. G. Veltman, Nucl. Phys. **B160**, 151 (1979).
[36] T. Hahn and M. Perez-Victoria, Comput. Phys. Commun. **118**, 153 (1999).
[37] G. J. van Oldenborgh and J. A. M. Vermaseren, Z. Phys. C **46**, 425 (1990).
[38] K. Hartling, K. Kumar, and H. E. Logan, Phys. Rev. D **91**, 015013 (2015).
[39] V. Khachatryan *et al.* (CMS Collaboration), Eur. Phys. J. C **75**, 212 (2015).
[40] G. Aad *et al.* (ATLAS Collaboration), Eur. Phys. J. C **76**, 6 (2016).
[41] C.-W. Chiang, S. Kanemura, and K. Yagyu, Phys. Rev. D **90**, 115025 (2014).
[42] A. Arhrib, R. Benbrik, M. Chabab, G. Moultaka, M. C. Peyranere, L. Rahili, and J. Ramadan, Phys. Rev. D **84**, 095005 (2011).
[43] M. Aoki and S. Kanemura, Phys. Rev. D **77**, 095009 (2008); **89**, 059902(E) (2014).
[44] G. Tavares-Velasco and J. J. Toscano, Phys. Rev. D **65**, 013005 (2001).
[45] T. Inami, C. S. Lim, B. Takeuchi, and M. Tanabashi, Phys. Lett. B **381**, 458 (1996).
[46] G. Gounaris *et al.*, arXiv:hep-ph/9601233.
[47] R. Mertig, M. Bohm, and A. Denner, Comput. Phys. Commun. **64**, 345 (1991).